Potential of metal monoliths with grown carbon nanomaterials as catalyst support in intensified steam reformer: a perspective

Luqmanulhakim Baharudin[a], Alex Chi-Kin Yip[a], Vladimir Golovko[b] and Matthew James Watson[a,*]

[a]Department of Chemical and Process Engineering, College of Engineering, University of Canterbury, Private Bag 4800, Christchurch 8140, New Zealand

[b]School of Physical and Chemical Sciences, College of Science, University of Canterbury, Private Bag 4800, Christchurch 8140, New Zealand

* *Corresponding author*. Tel.: +64 3 369 3803

E-mail address: matthew.watson@canterbury.ac.nz (Matthew James Watson)

Keywords: carbon nanomaterials; metal monolith; process intensification; steam reforming; textural promoter

Abstract

A monolithic catalytic support is potentially a thermally effective system for application in an intensified steam reforming (SR) process. In contrast to ceramic analogues, metal monoliths exhibit better mechanical strength, thermal conductivity and a thermal expansion coefficient equivalent to that of the reformer tube. A layer of carbon nanomaterials grown on the metal monolith's surface can act as textural promoter offering sufficient surface area for hosting homogeneously dispersed catalytically active metal particles. Carbon nanomaterials possess good thermal conductivities and mechanical properties. The future potential of this system in SR is envisaged based on hypothetical speculation supported by fundamental carbon studies from as early as the 1970s and sufficient literature evidence from relatively recent research on the use of monolith and carbon in catalysis.

Thermodynamics and active interaction between metal particle surface and carbon-containing gas result in coke deposition on the nickel-based catalysts in SR. The coke is removable *via* gasification by increasing steam to carbon ratio to above stoichiometric but risks a parallel gasification of the carbon nanomaterials textural promoter, leading to nickel particles sintering. We present our perspective based on literature that under the same coke gasification conditions, the highly crystallized carbon nanomaterials maintains high chemical and thermal stability.

Graphical Abstract

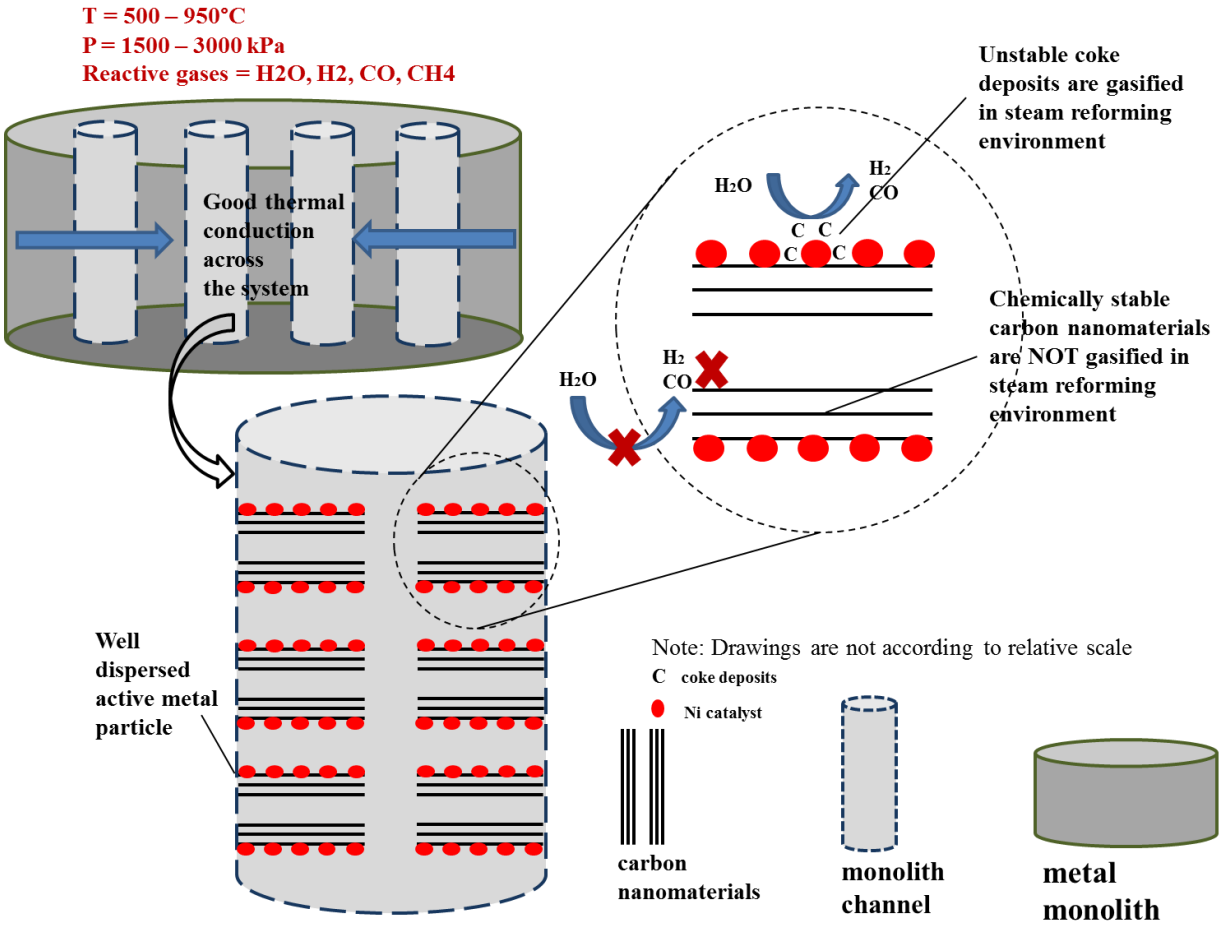

Graphical abstract: Excellent mechanical and thermal properties and chemical stability of carbon nanomaterials textural promoter on metal monolith withstand steam reforming conditions and enhance catalytic activity for improved reaction performance.

1. Introduction

Poor adhesion of inorganic oxide washcoating layer typically used to host the catalytically active metal particles on metal monoliths has been identified as a gap that raises the need to research an alternative textural promoter (Baharudin & Watson, 2017b). Works demonstrating growth of carbon nanomaterials for an application as a textural promoter on the surface of metals (Baird, Fryer, & Grant, 1974; Jitendra Kumar Chinthaginjala, Bitter, & Lefferts, 2010; J. K. Chinthaginjala & Lefferts, 2009; J. K. Chinthaginjala, Thakur, Seshan, & Lefferts, 2008; J. K. Chinthaginjala, Unnikrishnan, Smithers, Kip, & Lefferts, 2012; Jarrah, Li, van Ommen, & Lefferts, 2005; S. Pacheco Benito & Lefferts, 2010; Sergio Pacheco Benito & Lefferts, 2012; Tribolet & Kiwi-Minsker, 2005), ceramics (Morales-Torres et al., 2009; Zhu, Jia, Li, Lu, & Zhu, 2013), and graphite (P. Li et al., 2006) structured supports have inspired us to envision an application of this state-of-the-art knowledge in the field of chemical engineering by presenting our critical insights to its potential in a new development of a monolithic catalytic support technology for an employment in an intensified steam reforming process.

Process intensification, where the process volumes are reduced per unit volume of gas, has been given extensive attention in the chemical engineering field. There are two ways a process can be intensified. First, multiple unit operations are combined as a single operation; and second, a process unit size is reduced. Both ways offer cost and weight savings as a benefit, and additionally, the latter also exhibits a better thermal response to transient behaviour as a result of a smaller amount of energy required to heat the smaller process unit (Giroux, Hwang, Liu, Ruettinger, & Shore, 2005). Process intensification is especially useful for supplying hydrogen for fuel cell technologies, where a compact reformer design is required to provide the distributed hydrogen supply infrastructure. This makes refueling a hydrogen powered automotive fuel cells convenient, as the on-site generation of hydrogen eliminates the need for the distribution logistics along the supply chain (Barreto, Makihira, & Riahi, 2003; Dincer, 2002).

In an industrial steam reformer, the reaction takes place in the reformer tubes containing a bed of randomly packed pelletized nickel-containing catalysts (Xu & Froment, 1989). Nickel has not only been used in the steam reforming for decades (Jones et al., 2008), but is also the most frequently used due to its satisfactorily high activity at a substantially lower price due to its

abundant availability in comparison with other metals (Guo, Sun, Yu, Zhu, & Liu, 2012; Wu et al., 2013).

A large temperature gradient is generated by the flow of heat from the reformer tube wall radially inward toward the catalyst bed's center in an industrial scale steam methane reformer due to the highly endothermic nature of the reaction. The gradient is notably steeper at higher feed rates as a result of the catalyst becoming more active while the thermal conductivity remains low (Roh, Lee, Koo, Jung, & Yoon, 2010). A large amount of heat necessary for the steam methane reforming (SMR) reaction over the commercial pelletized Ni/alumina catalyst is supplied externally at high temperatures. However, the heat transport is limited in such a way that large areas of reformer tube are required, and hence a bigger catalyst volume. This consequently affects the reaction performance (Ryu et al., 2007).

The limitation in the current reformer design at an industrial scale lies within the reformer tube diameter, where a calculated safety factor must be imposed to eliminate the risks of temperature runaway, where a certain minimum flow rate of the process gas per tube radius is typically required for preventing hot spots (Tronconi, Groppi, & Visconti, 2014). Therefore, for an overall increase in the system's thermal efficiency, a significant improvement in the radial heat transfer is required for a higher energy utilization (Tonkovich et al., 2004), so that a possibility of enlarged reformer tube diameters can be introduced.

A monolithic-supported catalyst has the potential in overcoming the challenges of heat transport in an industrial SMR operation employing a packed pellet-supported catalyst bed (Baharudin & Watson, 2017b), which also finds a potential in materializing the concept of a compact reformer that supports process intensification initiative. In this article, our review revolves around two main discussions. The first is the monolithic structure itself where its design considerations for an application in steam reforming operation are presented. This however covers a small part of the overall scope of this article, as a comprehensive review of this subject has already been presented in our earlier article (Baharudin & Watson, 2017b). Based on the same article, before the end of the first part, an analysis on an area where a current gap is identified towards materializing the application of the monolithic catalytic support in the steam reforming is discussed, where we reiterate the poor adhesion of inorganic oxide washcoating layer on metal monoliths as the gap that needs an address.

In the second main discussion of this article, we present our perspective on the potential of growing carbon nanomaterials on metal monoliths as the alternative textural promoter. An analysis of the properties of the carbon nanomaterials that suit the steam reforming operation is presented. We also note that the nickel-based catalyst in steam reforming operation is susceptible to coke deposition due to thermodynamics and active interaction between the metal particle surface and the carbon-containing gas. The challenge in the industrial reforming operation of preventing the deposition of undesired carbon coke on the internal reformer tube is real, as it threatens the lifetime of the tube due to formation of hot spots.

To justify our perspective on the potential of the carbon nanomaterials in this particular application, we analyse coke formation as a common problem in steam reforming, regardless of the substrate materials used as the catalyst supports; be it inorganic oxides or carbon nanomaterials. We also discuss steam reforming *operando* conditions under which coke formation can be avoided and the conditions under which the coke deposits, if formed, are removed by gasification. Efforts to remove the laydown via coke gasification by increasing the steam to carbon ratio to above stoichiometric however introduces a risk of parallel gasification of the carbon nanomaterials used as the textural promoter. We present our perspective based on literature that under the same conditions needed for coke gasification, the textural promoter in the form of high purity, highly crystallized carbon nanomaterials still maintains high stability and is not simultaneously gasified with the disordered, more reactive coke. In summary, based on our hypothetical speculation supported by fundamental carbon studies dated back from as early as the 1970s and sufficient literature evidence from relatively recent research on the use of carbon in catalysis, we present our envision on the future potential of metal monoliths with grown carbon nanomaterials as catalyst support in steam reformer.

2. Monolithic structure

A monolithic structure is made of a single structure with thin-walled narrow channels parallel to each other (Ronald M. Heck, Gulati, & Farrauto, 2001; Roy, Bauer, Al-Dahhan, Lehner, & Turek, 2004; Zamaniyan, Khodadadi, Mortazavi, & Manafi, 2011) which result in a low resistance to the flow of the reactants (Ryu et al., 2007) and hence, a pressure drop reduction by one to two orders of magnitude compared to that of randomly packed pellets (Ryu et al., 2007; Zamaniyan et al., 2011). The monolithic support offers the benefits of keeping the

pressure drop to the minimum when operating at the high throughput (Ryu et al., 2007) without hydrodynamic instability issues (Roy et al., 2004). A lower pressure drop translates to a lower operation energy loss (Ronald M. Heck et al., 2001; Zamaniyan et al., 2011), and hence, improves the efficiency of the system's energy utilization (Roy et al., 2004).

In an industrial SMR operation, an improved reaction performance and an efficient hydrogen production can be achieved as a result of the monolithic system's capability to reach nearer approach-to-equilibrium of the reforming reaction at the reformer exit, and hence, get close to complete methane conversion (Mohammadzadeh & Zamaniyan, 2002). In heterogeneous gas-solid catalytic reactions, increasing the specific surface area and uniformity of flow distribution of the process gas through the monolithic catalytic system will enhance both the mass and the heat transfer effectiveness, thereby reducing the size of the reactor and therefore, process intensification.

Therefore, in a compact reformer, the monolithic catalytic system can introduce a prospect of heat transfer enhancement across the catalyst bed and an improvement in the accessibility of the catalytically active sites to the reactants. This has been demonstrated by Roh et al. (2010) in a small-scale reformer design, where the temperature of the catalysts bed was high enough for the reaction to take place in a reduced volume. This can potentially bring down the capital investment and increase the production throughput, which corresponds to an investment costs reduction. Zamaniyan et al. (2010) introduced a bulk monolithic catalyst, where the monolithic body is made of intrinsically active material for natural gas reforming, as an alternative to the packed bed layout. It was demonstrated that the former exhibited a higher mechanical strength. The outcome of this investigation introduced the benefit of having the frequency of reformer shut down and start up for replacing broken catalysts reduced or avoided, and hence, minimizing the operating costs.

2.1 Honeycomb *vs.* Foam

The honeycomb monolith's structure is geometrically defined by cells-per-square-inch (CPSI), which is a key parameter for pressure drop and mechanical strength. It is determined collectively by the number of channels and their diameter (d_{ch}), and the void fraction (ε) of the structure termed as open frontal area (OFA) (Ronald M. Heck et al., 2001; Zamaniyan, Mortazavi, Khodadadi, & Manafi, 2010). Selectivity is mainly governed by temperature in

numerous reactions in the chemical plants. However, the temperature control is difficult as radial mixing is not possible because the segregated flow in the parallel channels of the honeycomb monoliths makes the structures behave like an adiabatic reactor.

Structures like foam, made by solid struts connecting the spherical-like cavities (the cells) through openings or windows (the pores), offer a solution to this shortcoming as the radial mixing is made possible in the open-celled foam structures. This prevents non-uniform distributions of the reactants over the reactor's cross section. The temperature gradients in the radial and axial directions in non-adiabatic reactors can be reduced with the continuous thermally-connected structure of the foams, in comparison to the honeycomb monoliths. As a result, the radial heat transfer is further enhanced and the possibility of hot spots is curtailed in the foam structures (Ronald M. Heck et al., 2001). Figure 1 shows the geometrical identification of the honeycomb monoliths and foams.

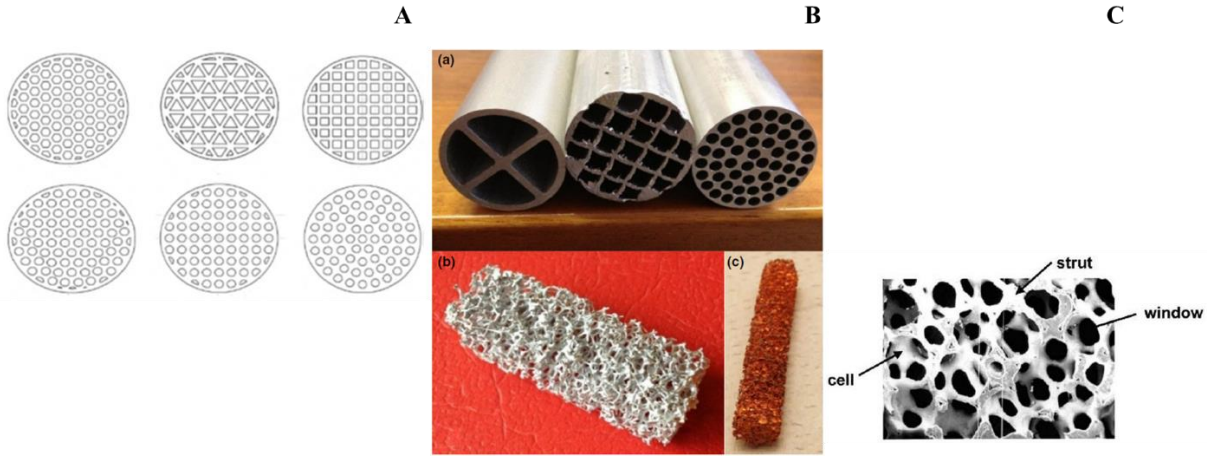

Figure 1: Geometries of honeycomb monoliths and foams; A: Various shapes and arrangements of channels of honeycomb monolith (Zamaniyan et al., 2010). Reproduced with permission from Elsevier, B: Example of (a) aluminium honeycomb monoliths, (b) aluminium foam, (c) copper foam (Tronconi et al., 2014). Reproduced with permission from Elsevier, C: Geometrical identification of a foam structure (Twigg & Richardson, 2002). Reproduced with permission from Elsevier.

The monolith needs to also contain sufficient active catalytic sites for the desired conversion efficiencies (Ronald M. Heck et al., 2001). However, the amount of catalyst deposited on the honeycomb monoliths' walls of a given volume is a lot less than that on small pellets. The foams, which possess open accessible pores in the range of 10 to 100 unit per inch with an interconnecting porosity typically in the range of 75 to 90% or higher, provide the surface for the catalytic components' loading (Tronconi et al., 2014; Twigg & Richardson, 2002). The

interaction between the reactants and the catalysts coated on the foam struts is also enhanced by the high surface area per unit volume of the structure (Tronconi et al., 2014). Although the surface areas per unit volume of a monolith and an open cell foam can be, in some cases, comparable, a key role in heat and mass transfer is played by the flow path throughout the structures. The open foam structure in overall introduces more tortuous flow paths compared to the straight monolith channels. Such a higher tortuosity forces the fluid to get in close contact with foam struts, thus enhancing the fluid-solid interaction.

Even though the foams are a better structure than the honeycomb monoliths for the application in steam reforming, the derivation of reliable engineering correlations for the prediction of the heat and mass transfer resistances in the foam structure that is of uneven surface and geometries, remains a challenge (Tronconi et al., 2014). A recent article by Fee (2017) brings a fresh hope to overcome this challenge through the use of 3-dimensional printing (3DP) technology in the design and fabrication of a porous structure. The 3DP technology allows fabrication of structures with accurate geometries that have been optimized through computational fluid dynamics, where the seamless transition between digital data and physical objects enables the gap between theory and experiment to be closed through experimental investigation of the properties of the 3DP-fabricated structures. Structures of the same geometries but fabricated by different substrate materials that have different properties such as thermal conductivity can conveniently be experimentally evaluated. Parra-Cabrera et al. (2018) provides a comprehensive review on research work in the design and construction of reactors and structured catalysts using computational modeling and 3DP.

In the article by Fee (2017), a concept of "mesostructure" has been introduced, which refers to a uniform porous structure comprising identical solid and fluid phase geometries. The concept allows a controlled design of a so-called "defined foam structure" known as periodic open-cellular structures (POCS) where a control over the geometries such as size and shape is made possible to be printed.

A mathematically defined equation for POCS design is given by (Fee, 2017):

$$\sin(x)\cos(y) + \sin(y)\cos(z) + \sin(z)\cos(x) = t \qquad (1)$$

An alteration of the value of *t* allows a tuning of the relative volume fractions of the solid and fluid phases, which in turn provides a control over the porosity and relative dimensions of the two phases. Eq. (1) also provides a systematic means to distort the structure along any of the coordinates with an addition of scalar multipliers to their relevant terms on the left-hand side. Figure 2 shows a computer-aided design of such an example of a mesostructure.

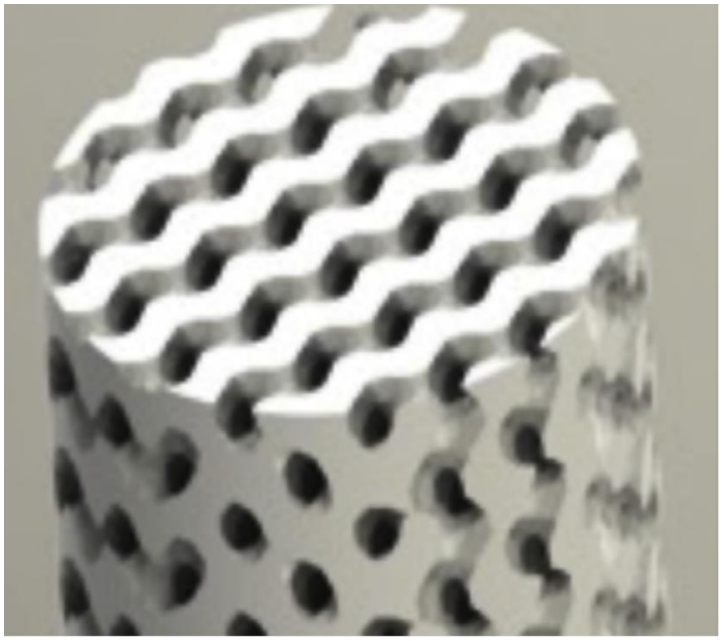

Figure 2: Example of a defined porous structure (mesostructure) (Fee, 2017). Reproduced with permission from Elsevier.

Various POCS structures have been demonstrated as structured reactors that exhibited benefits of a better control on the transport processes such as the fluid flow and distribution, heat transport and pressure drop. Among other examples include the investigation of POCS for intensification of multiphase reactors (Lämmermann, Horak, Schwieger, & Freund, 2018), as catalytic reactors for heat transfer intensification (Busse, Freund, & Schwieger, 2018) and as catalyst supports for an effective gas-liquid distribution (Lämmermann, Schwieger, & Freund, 2016).

For a honeycomb monolithic structure, presented next are the engineering correlations for designing its geometries in a systematic approach for an employment in the steam reformer. Using these correlations, a honeycomb monolithic structure of minimal mass and heat transfer

resistances can be designed at an optimal balance with minimal pressure drop and satisfactory mechanical strength.

2.1.1 Mass transfer

Two established types of mass transfer limitations in a monolithic catalytic structure are:

i) bulk (external) mass transfer of process gas to the monolithic structure's surface;
ii) diffusion of reactants through the monolith's microporous structure to the catalytically active metal sites.

2.1.1.1 Process gas bulk flow

The shape, size, and arrangement of the monolith's channels are optimized using mass transfer fundamental parameters for a required reaction conversion, by assuming a bulk mass transfer limited reaction, so that the overall reaction kinetics are dominated by the effect of mass transfer (Ronald M Heck, Farrauto, & Gulati, 2009). The optimized geometries in a bulk mass transfer limited regime are crucial in facilitating a uniform velocity and composition of the process gas inlet flow within each channel (Giroux et al., 2005).

A material balance across a plug-flow reactor assuming one-dimensional steady-state and isothermal operation at low conversion (Ronald M Heck et al., 2009):

$$v\frac{dC}{dz} = -r \qquad (2)$$

where

v = velocity of reactant

C = molar concentration of reactant

z = length of reactor

r = molar rate of reaction

Solving eq. (2) for the reaction conversion (X) by integration along the reactor length (z), applying the mass transfer dimensionless numbers, yields:

$$X = 1 - exp\left[-\frac{(Sh_{\mathrm{ch}}\, a/\varepsilon\, L)}{(Sc_{\mathrm{monolith}}\, Re_{\mathrm{monolith}})}\right] \quad (3)$$

where

Sherwood number in monolith's channel, $Sh_{ch} = K_g\, d_{ch} / D_{AB}$

Schmidt number of monolith, $Sc_{monolith} = \mu / (\rho\, D_{AB})$

Reynolds number of monolith, $Re_{monolith} = (W / A\, \varepsilon).d_{ch} / \mu$

K_g = mass transfer coefficient of reactant

a = geometric surface area per unit volume of monolith

L = length of monolith

W = total mass flow rate of the process gas to the catalytic wall of monolith's channel

A = frontal area of monolith

d_{ch} = diameter of monolith's channel

ε = void fraction of monolith

D_{AB} = diffusivity of the reactant in monolith's channel

ρ = process gas density at operating conditions

μ = process gas viscosity at operating conditions

A monolithic structure of an optimized CPSI can be designed using eq. (3), for the highest possible conversion. In order to achieve this, the term $\frac{(Sh_{\mathrm{ch}}\mathrm{a}/\varepsilon\,\mathrm{L})}{(Sc_{\mathrm{monolith}}\,Re_{\mathrm{monolith}})}$ in eq. (3) should be as large as possible, where the parameter a should be maximized by maximizing the channel diameter, d_{ch} and the number of channels, and minimizing the monolith's length, L. However, the trade-off balance with the structure's mechanical properties such as Young's modulus, E-modulus, fatigue, and tensile and compressive strength (Ronald M. Heck et al., 2001) needs to be taken into consideration.

2.1.1.2 Diffusion of molecules in the pores

The diffusion of reactants within the catalytic washcoat layer (M. Saito, Kojima, Iwai, & Yoshida, 2015) is imperative and especially critical for the SMR reaction, which is a diffusion-limited reaction (Zamaniyan et al., 2011). The intra-phase (internal) mass transfer resistance is characterized as effectiveness factor:

$$\text{Effectiveness factor} = \frac{\text{Mean rate of reaction within the catalytic washcoat layer}}{\text{Rate of reaction at the external surface of the washcoat layer}} \qquad (4)$$

The washcoat material selection of high surface area needs careful attention for achieving active phase dispersion homogeneity and uniformity (Mohino, Martin, Salerno, Bahamonde, & Mendioroz, 2005).

2.1.2 Heat transfer

A bare monolith structure ($k_{S,R}$) made of a material of thermal conductivity (k_S) with void fraction, ε has an effective radial conductivity of (Boger & Heibel, 2005; Groppi & Tronconi, 1996; Tronconi et al., 2014):

$$k_{S,R} = k_S \left(\left(1 - \sqrt{\varepsilon}\right) + \frac{\sqrt{\varepsilon}}{\left(1 - \sqrt{\varepsilon} + \frac{k_G}{k_S}\sqrt{\varepsilon}\right)} \right)^{-1} \quad (5)$$

where

(k_G) = thermal conductivity of process gas

The heat transfer by convection of process gas flowing inside the channels to/from the channel wall is given in the form of a heat transfer coefficient (h_{GS}) and the corresponding Nusselt number of the channel (Nu_{ch}) (Boger & Heibel, 2005):

$$h_{GS} = \frac{Nu_{\mathrm{ch}} k_G}{\mathrm{d_{ch}}} \quad (6)$$

where

$$Nu_{\mathrm{ch}} = 0.571 \left(Re_{\mathrm{ch}} \frac{\mathrm{d_{ch}}}{\mathrm{L}} \right)^{2/3} \quad (7)$$

for a laminar flow inside a small-hydraulic-diameter a channel, with Re_{ch} = Reynolds number of the process gas flowing inside the channel.

An optimized heat transfer coefficient (h_{GS}) can be achieved by maximizing the void fraction of the monolith, ε through an optimization of the channel wall shape and size (maximizing $\mathrm{d_{ch}}$ will minimize channel wall, which in turn improves the heat flux improvement and reduces the thermal resistance), without jeopardizing the monolith structure's mechanical properties.

2.1.3 Pressure drop

The OFA of the monolithic structure must be large enough to create little flow resistance, and hence, lower pressure drop. The pressure drop (ΔP) across the monolithic structure along its

axial direction derived from an energy balance is: (Ronald M Heck et al., 2009; Ronald M. Heck et al., 2001):

$$\Delta P = \frac{2 f L \rho v_{ch}^2}{d_{ch}} \quad (8)$$

where

f = dimensionless friction factor
v_{ch} = velocity in monolith's channel = W / (ρ A ε)

Eq. (8) is useful for the purpose of evaluating the options of various monolith structures of different cell densities, wall thicknesses and channel diameters, to suit other plant design constraints, for example, space and compressor capacity (Ronald M. Heck et al., 2001). Similarly to what has been seen in eq. (3), the pressure drop is minimized for achieving the highest possible conversion by maximizing the channel size, d_{ch} and minimizing the monolith length, L.

2.2 Metals *vs.* Ceramics

The most common substrate materials used for manufacturing the monolith support structures are ceramics and metals. The example of an existing ceramic honeycomb monolithic structure is the catalytic converter installed in vehicles. The substrate used is cordierite ($2MgO\ 2Al_2O_3\ 5SiO_2$), an extruded multi-cell ceramic of low thermal expansion and high resistance to thermal shock fracture (Ronald M. Heck et al., 2001). Honeycomb monoliths have also been commonly fabricated using metals like iron/chromium alloy, FeCralloy (Fe 72.8/Cr 22/Al 5/Y 0.1/Zr 0.1). Both the cordierite and the FeCralloy exhibit excellent resistance to oxidation at high temperatures (Giroux et al., 2005).

In the overall design of fabricating a monolithic catalytic support, a comparative analysis based on literature findings by Baharudin & Watson (2017b) reveals that metals are a better substrate than ceramics for fabricating the monolithic support in a structured steam reforming reactor due to their mechanical strength, good thermal conductivity and equivalent coefficient of thermal expansion (CTE) with the reformer tube material. Metal offers a greater possibility of fabricating a monolith structure of thinner walls with an OFA of up to 90% (Ronald M. Heck et al., 2001), which allows for bigger d_{ch} and hence, lower pressure drop.

A material does not only rely on its good thermal properties for a great heat transfer performance. It also depends on its available contact surface area. The monolith needs to contain sufficient active catalytic sites for the desired conversion efficiencies (Ronald M. Heck et al., 2001). However, metals in general do not possess sufficient external surface area for the purpose of making it a good substrate for a catalyst support. One way to overcome this issue is by using high surface area structures such as fins, corrugated foils, foams and felts, which are also capable of inducing turbulence within the process gas flow. For an application in the context of our discussion, a metallic foam is an attractive porous material as it possesses pores of diameter of around 0.5 mm that leads to low viscous losses, a high porosity (~95%) that creates a relatively large specific surface area of around 1 m^2/g, and definitely, a good thermal conductivity (Tuzovskaya et al., 2012).

Another way of introducing high surface area on the metal structures is by adding a porous layer (Jitendra Kumar Chinthaginjala et al., 2010) onto the metal surface as a textural promoter. A synergistic effect on the increased specific surface area of the metal monolithic structure is introduced when both means are combined, whereby not only can the mass and heat transfer rates in the catalytic reactions be maximized, but a higher catalyst loading can also be achieved. To make the most effective monolithic catalytic structure, the above factors are combined where a more active catalytic component is deposited in the coating layer, at a higher loading amount (Giroux et al., 2005). To achieve this, the added porous layer coating the high-surface-area metal structure should also produce well dispersed metal catalyst nanoparticles on its surface for an efficient reaction, and be mechanically stable to withstand the high temperature gradient (Jitendra Kumar Chinthaginjala et al., 2010) in the SMR reaction. For more works concerning washcoating of complex geometry supports, a couple of references (Almeida et al., 2010; Nijhuis et al., 2001) can be useful.

3. Textural promoter on monolith surface

3.1 Inorganic oxide washcoating

Typically, the washcoating of the porous layer on the structured support surface is done by a deposition of an inorganic oxide layer that has the same textural properties as the conventional pelletized catalyst supports such as alumina and silica. However, the relatively low porosity and surface area of the metal in comparison to that of ceramic substrate results in poor adhesion of the conventional catalytic washcoating layer (Giroux et al., 2005; Ronald M. Heck et al., 2001). This disadvantage is identified as a gap in materializing the application of the monolithic catalytic system in steam reforming that takes place at high temperatures of up to around 950 °C (Mohammadzadeh & Zamaniyan, 2002; Zamaniyan et al., 2011) in a frequent heating and cooling cycle (Baharudin & Watson, 2017b).

Washcoating is defined as a procedure of coating a bare monolithic structure with a layer of a highly porous oxygenated carrier with the objectives of enhancing the structure's BET surface area as well as facilitating the traverse diffusion of the gaseous reactants/products to/from the active catalytic component (metals or metal oxides) dispersed in its micropores or on its surface, for an effective process gas–catalyst interaction (Ronald M. Heck et al., 2001; Nijhuis et al., 2001).

3.1.1 Washcoating of ceramic structures

In a monolithic structure made of ceramics, the catalytic washcoating of its surface can be done via two approaches; first by filling the high surface area washcoat material into the macropores of the monolith, and second by depositing a layer of the washcoat material on the overall surface of the monolithic structure whereby the structure's macropores anchor the washcoat layer (Nijhuis et al., 2001).

Nijhuis et al. (2001) in their review article presented the steps involved in the preparation of the inorganic oxide washcoating solutions explicit to their corresponding washcoating techniques and principles; namely colloidal solutions coating, sol–gel coating, and slurry coating, for washcoating specifically cordierite monoliths. In our present context of discussion, the list of techniques presented by Nijhuis et al. (2001) may not be adoptable in the case of metal monoliths due to the significantly different morphology of the two substrate materials in terms of their surface porosity. Ceramic substrate have the advantage of possessing a highly porous surface that can promote strong anchoring with the washcoat layer, while metals suffer from the lack of this desired property (Baharudin & Watson, 2017b). In addition, even with the surface porosity advantage of the ceramic monoliths, the inorganic oxide washcoat layer sometimes may still suffer from adhesion issues on the structure's surface if the preparation of the washcoat solutions is not properly taken care of or prepared incorrectly. This makes the aforementioned washcoat layer materials and techniques even more unsuitable for an application using metal monoliths.

3.1.2 Washcoating of metal structures

The properties of the structure's substrate material that are crucial for strong adhesion of the catalytic washcoating layer are its surface roughness and compatibility with the washcoat material (Echave, Sanz, Velasco, Odriozola, & Montes, 2013). On the metal monoliths, a pretreatment step is included in a typical washcoating procedure to ensure a good bonding with the washcoat layer (Basile et al., 2008; Echave et al., 2013; Ronald M. Heck et al., 2001). The pretreatment (activation) includes thermal oxidation, anodization or chemical treatments (Echave et al., 2013), followed by calcination in air flow at certain temperatures after the washcoating step (Ronald M. Heck et al., 2001). A review article by Montebelli et al. (2014) serves as a good reference for all the details concerning the activation of metallic supports.

However, even though the effect of poor washcoat layer adhesion due to inadequate surface roughness of the metal may be improved by the addition of the pretreatment steps, the non-equivalence of the two materials in the CTE could lead to a cracking of the washcoat layer and subsequent loosening and spalling of the catalytic metals/metal oxides (Basile et al., 2008)

especially in the steam reforming application that is subjected to thermal cycles (Baharudin & Watson, 2017b; Giroux et al., 2005).

3.2 Carbon nanomaterials growth

In overcoming the identified washcoat layer poor adhesion issue on monolithic structures made of metal substrates, we analyse the potential of growing carbon nanomaterials on the metal monoliths as an alternative to the inorganic oxide layer washcoating. Various works (Baird et al., 1974; Jitendra Kumar Chinthaginjala et al., 2010; J. K. Chinthaginjala & Lefferts, 2009; J. K. Chinthaginjala et al., 2008; J. K. Chinthaginjala et al., 2012; Jarrah et al., 2005; P. Li et al., 2006; Morales-Torres et al., 2009; S. Pacheco Benito & Lefferts, 2010; Sergio Pacheco Benito & Lefferts, 2012; Tribolet & Kiwi-Minsker, 2005; Zhu et al., 2013) reported in the demonstration of the growth of carbon nanomaterials directly on various types of monolithic structures, serve as evidence that not only can this novel material be a good potential alternative to the oxide washcoated layers; it can also be grown directly on the metal structure. Indeed, the formation of carbon filament layers on a structured material such as foam, monolith, or felt helps shorten the diffusion path length of the process gas (J. K. Chinthaginjala, Seshan, & Lefferts, 2007).

The closest hypothesis on the carbon nanomaterials' stability on a metal surface that we can make is based on a reported work by Abad et al. (2008). In their work, the tribological behaviour of carbon nanotubes (CNTs) grown by plasma enhanced chemical vapour deposition (PECVD) on a stainless steel coated with a layer of metallic cobalt nanoparticles was investigated under humid ambient air of 25 – 40 % relative humidity at room temperature using reciprocating ball-on-flat sliding. It was revealed that the friction coefficients over 200 cycles of growing loads (0.25 to 5 N) decreased to steady state values of around 0.1 – 0.2. The wear scars on the steel balls and the CNTs samples of the test at 0.25 N (200 cycles) were examined by optical microscopy. Only a thin layer of CNTs debris was seen on the ball after friction test, in comparison to another sample of CNTs grown directly on a stainless steel without the presence of a layer of metallic cobalt nanoparticles that showed a distinctive clear worn out of CNTs from the stainless steel structure surface.

The growth of carbon nanomaterials on the macroscopic monolith is a great challenge, especially in creating uniform growth conditions to cover the large monolith surface. The standard thermal chemical vapour deposition (CVD) would be quite good for carbon nanomaterials growth on the metal monolith as the monolith itself will conduct heat from external furnace into its inner parts. A demonstration of such a work was presented by Sano et al. (2012). A synthesis of multi-walled carbon nanotubes (MWCNTs) of high purity and uniformity at all locations in a stainless steel porous block was successfully achieved by activating the inner surface of the block by heat treatment at 800 °C in O_2–Ar environment, followed by reduction at 700 °C in H_2–Ar. A mixture of ethylene and Ar was then diffused into the pores for the ethylene decomposition to form the uniform MWCNTs.

Parthangal et al. (2007) presented a simple catalytic CVD (CCVD) technique to directly grow well-aligned arrays of CNTs at growth temperature of 625 °C using iron/alumina composite catalyst on a series of metal and metal alloy substrates. Of all the metallic substrates, NiCr is the structure of our interest for a discussion, in order to relate with its application as the monolith's substrate material in the steam reformer. The tubes in a commercial reformer are made of nickel chromium alloy steel for example, HK40 (Cr 25%, Ni 20%, and Co 4%) and IN519 (Cr 24%, Ni 24%, Nb 1.5%, and Co 3%) (Mohammadzadeh & Zamaniyan, 2002). The outcome of the study by Parthangal et al. (2007) provides a meaningful analysis of the CNTs growth on the NiCr, as this metal alloy substrate possesses compatible CTE with the reformer tubes material where both expand and contract to the similar extent during heating and cooling in the reformer operation.

In Parthangal et al. (2007), the procedure employed involved micropipetting an aqueous solution of equal concentration of iron nitrate and aluminium nitrate onto the substrate structure to disperse the Fe/Al_2O_3 composite catalyst nanoparticles. The catalysed structure was then dried at room temperature, followed by a treatment in a mixture of $Ar\text{-}H_2$ flow in a tubular furnace at 625°C, prior to submission to a flow of acetylene at the same temperature for the nucleation and growth of the CNTs. The scanning electron microscopic (SEM) images revealed the growth of uniform and vertically well-aligned CNTs arrays at positions wherever the catalyst particles were dispersed. In comparison to the array of CNTs grown on a steel substrate, the adherence of the filamentous carbon layer was so weak that the filament was

readily peeled off the steel surface, but not on the NiCr surface. No CNTs adhesion strength test was reported in their work for us to provide an insight on the CNTs' stability on the NiCr structure's surface grown by the demonstrated technique, if employed in the steam reforming.

The PECVD technique is also capable of synthesizing uniform CNTs growth. The technique allows for good control of a surface-bound growth of a CNTs with the desired quality and uniformity on a substrate surface (Berenguer et al., 2009; Geng et al., 2004). Berenguer et al. (2009) demonstrated the growth of CNTs on a structured substrate using colloidal catalysts by employing this technique. Catalyst precursors in the form of colloidal nanoparticles are useful in catalysis applications to grow the CNTs on the surfaces of three dimensional (3D) complex monolithic structures, even with uneven geometries. Using PECVD method, a dc discharge current of 20 – 40 mA was generated by employing a voltage of 800 V between the sample heater and the gas inlet, with acetylene as the carbon precursor. The result was an abundant production of vertically aligned MWCNTs that covered almost the entire surface of the substrate, with generally well crystallized tubes, although there were also some defects observed in the graphitic structure.

In their work, Berenguer et al. (2009) presented the preparation of colloidal catalyst precursors with a narrow size distribution for achieving good control of the structural type of carbon nanomaterials formed. They reported the synthesis of a stable bimetallic Co/Pd colloidal catalyst for growing the carbon nanomaterials, with a demonstration of a successful formation of vertically aligned non-bundled forests of CNTs grown from the Co/Pd colloids.

Earlier to the work by Berenguer et al. (2009), several disadvantages of using the metal colloidal nanoparticles were identified by Geng et al. (2004). Their manipulations in an attempt to control the size distribution of the particles are often difficult, and hence may limit the production of uniform carbon nanotubes on a large monolith, as the metal colloidal particles are normally sensitive to air. The work presented Geng et al. (2004) would be a potential alternative method to overcome the problem of instability in air of the metal colloid by demonstrating the use of nickel formate as the catalyst precursor, taking advantage of not only its stability in the air but also its commercial availability at low cost. Nickel formate was demonstrated to be suitable for a surface-bound growth of MWCNTs on a SiO_2/Si structure, where the formation of the Ni nanoparticles was done *in situ* via thermal decomposition of the nickel formate precursor during the growth process of the carbon nanotubes. The self-redox

reaction of the nickel formate resulted in decomposition of the formate directly to metallic Ni particles without the formation of nickel oxide, and hence, the requirement for the activation of the catalyst particles *via* reduction in the presence of hydrogen, was eliminated.

The substrate material of the monolith also plays a role in determining the uniformity of the CNTs grown on it. Duy et al. (2009) studied the growth of CNTs on Ni-coated stainless steel substrates (NiFe, NiCr) and Ni-coated silicon substrates ($NiSi_2$) by dc PECVD and found that the diameter of the CNTs grown on the former was more uniform, which was be due to the uniformity in the size of the Ni particles on the stainless steel substrates. The deposition of the Ni layer and a TiN buffer layer of thickness of 50 and 1000 Å respectively was performed using a radio-frequency magnetron sputtering system on both the substrate types. The Ni activation was done by an introduction of NH_3 gas for 6 min to create uniform Ni particles, followed by annealing procedures at 600 °C in H_2, forming Ni grains. The growth of the CNTs took place at 600 °C for 15 min by decomposition of acetylene in ammonia carrier.

Other than PECVD, another modified CVD technique that has the potential to be adopted for synthesizing the uniform carbon nanomaterials on the 3D structures is pulsed pressure chemical vapour deposition (PPCVD). This technique has been extensively employed in the manufacturing of thin films deposition and coatings on large surface areas for various applications. Examples include the growth of titania (TiO_2) film layers on nickel substrates (S. Krumdieck & Raj, 1999; S. Krumdieck & R. Raj, 2001; S. P. Krumdieck & R. Raj, 2001) and on patterned Si and silicon nitride (SiN) substrates (Siriwongrungson, Alkaisi, & Krumdieck, 2007); and zirconia films deposited on metal, alumina and porous nickel cement substrates (S. P. Krumdieck, Sbaizero, Bullert, & Raj, 2002) and on various solid and porous substrates (S. Krumdieck, Kristinsdottir, Ramirez, Lebedev, & Long, 2007).

Even though there has not been any work on synthesizing carbon nanomaterials by this method published in the literature, the PPCVD technique is promising for an adoption in growing the carbon nanomaterials on the 3D substrates. CNFs growth on a structured surface by this technique has been demonstrated in the laboratory of the Department of Mechanical Engineering, University of Canterbury. Principally, PPCVD is a non-catalytic CVD process. The carbon precursor gas is supplied from a high pressure source, which flows through a supersonic choked orifice, to the evacuated CVD reactor where the 3D substrate is placed, during a short 0.4-second injection. Rapid diffusion of the carbon precursor to the substrate

takes place, followed by the thermal decomposition of the precursor, where the carbon nanomaterials are formed on the substrate. The pressure in the reactor reaches 800 Pa at the termination of the injection, and reduces to 30 Pa during a 20-second pump-down phase by a vacuum pump. The resulting carbon nanomaterial length can be controlled by repeating the pulse cycles until the desired length is reached.

4. Properties of carbon nanomaterials as a textural promoter candidate for steam reforming

An analysis of the properties of the carbon nanomaterials that suit the steam reforming operation is presented here. In general, the fundamental role of the support in a catalytic system is to keep the active catalytic particles in a well dispersed state. A good catalyst must have high surface area and it has to be stable and sufficiently strong mechanically. An advantage offered by a highly porous support material is the ability to spread and disperse well the active metal catalyst phase throughout the pore system. Hence obtaining a large surface area per unit weight of active catalyst particles is possible.

A good catalyst support facilitates the external mass transfer of the process gas in the reactor to the surface of the catalyst support, and more importantly, it eases the internal mass transfer of the reacting system, where reactants and products counter-diffuse into and out of the pores of the catalyst support, to and from the catalytically active phase. This carries the benefits of improving the reaction heat dissipation, retarding the sintering of the active metal catalyst, and increasing the catalyst's resistance to poison.

The selection of the support is therefore important and must be based on desirable characteristics such as good stability under reaction conditions; satisfactory mechanical properties; and high surface area and porosity per unit volume (Rodríguez-reinoso, 1998). In this section, the properties of a filamentous carbon layer are reviewed to analyse its potential as a substitute to the washcoating layer in overcoming the lack of available surface area and poor adhesion on the metal structures. Based on our review of the properties as presented below, the structural form of the carbon nanomaterials should be an important specification if

one wishes to take advantage of the properties of this novel material in the application of energy intensive heterogeneous reactions of gas-phase reactants and products.

4.1 Surface textural properties

Carbon nanomaterials have porous properties that are principally governed by their texture, defined by the anisotropic hexagonal layers' degree of orientation (Beguin, 2006). In general, aggregates of entangled carbon nanomaterials (at times referred to as interwoven nanomaterial layer (Morales-Torres et al., 2009)) provide reasonably high surface areas of 100 – 200 m^2/g. This makes the carbon nanomaterial layer a potential candidate as a surface textural promoter on a metal monolith to enhance the structure's external surface area. In addition, the nanomaterials possess low tortuosity, high meso- and macro-porosity in the absence of micropores (J. K. Chinthaginjala & Lefferts, 2009; J. K. Chinthaginjala et al., 2008; Jarrah et al., 2005; Morales-Torres et al., 2009), which is the kind of porosity that is being sought after in many reactions for effective internal diffusion of reactant and product molecules to the active metal sites. They also possess high specific pore volume in the range of 0.5 – 2 cm^3/g (Jarrah et al., 2005).

These textural properties are desirable in a catalyst support material as they provide sufficient surface area to maximize the effective diffusion coefficient (Jarrah et al., 2005) and minimize the internal mass transfer limitations within the thin filamentous layers (J. K. Chinthaginjala et al., 2008). Due to the presence of mesoporous texture and large external surface area in the filamentous carbon, the resistance to inner pore diffusion of the reactants or the products could be considerably reduced during catalytic reactions. This has the possibility to dampen the effects of catalyst deactivation by the formation of coke molecules in the pores (P. Li et al., 2006), which is a vital feature in energy intensive reactions.

4.2 Thermal and chemical stability

The filamentous carbon layers also serve as an excellent candidate for catalyst supports due to their properties such as good resistance to oxidation (Morales-Torres et al., 2009); exceptional structural strength even under acidic environments (J. K. Chinthaginjala et al., 2008) despite their surface chemistry properties may be altered due to modification, addition or elimination of certain functional groups; and stability towards sintering avoidance for an application in high-temperature gas reactions (J. K. Chinthaginjala et al., 2007). Thermogravimetric analysis (TGA) reveals that different structural forms of carbon exhibit different levels of stability (Datsyuk et al., 2008; Moraes et al., 2011).

In an inert environment such as in helium, argon or nitrogen flow, the thermal stability of the carbonaceous materials depends solely on their morphology and graphitic structure or crystallinity. In a reactive environment such as in the presence of hydrogen, steam and oxygen, the stability of the carbon depends on the thermal condition (operating temperature) and the chemical reactivity of the process gas on top of the different degree of carbon crystallinity. In the reactive gases, carbon has the tendency to be reactive at above certain temperatures that they become gasified and yield methane or carbon monoxide. In an oxygen flow, the disordered (amorphous) carbon has the tendency to get oxidized under mild conditions of approximately 500 °C due to its high density of defects, whereas temperatures of 600 °C or higher are required to combust the well graphitized carbon structure due to a higher activation energy requirement (Datsyuk et al., 2008; Moraes et al., 2011). In an inert, non-reacting gas flow, the thermal stability of the carbonaceous materials is expected to be better as compared to one in the presence of oxygen, in that a much higher temperature is required to gasify the carbon, and the gasification temperature increases with the level of carbon crystallinity.

One of the typical steps in a catalyst synthesis procedure is the calcination process, where a thermal treatment is conducted by subjecting the prepared catalyst to a gas flow at a certain temperature in order to improve the interaction between the metal active particles and the support, for an enhanced metal dispersion. In the previous works on the synthesis of the catalysts made of the metal nanoparticles deposited on the carbon nanomaterials support, the

calcination was reported to have taken place in a nitrogen flow at 350 – 400 °C for 2 – 3 hours (Abbaslou, Tavassoli, Soltan, & Dalai, 2009; López, Kim, Shanmugharaj, & Ryu, 2012; Shaikhutdinov, Avdeeva, Novgorodov, Zaikovskii, & Kochubey, 1997), or in an air flow at 350 °C for 1 – 4 hours (Mierczynski et al., 2016; Oliveira, Valençaa, & Vieirab, 2015; H.-M. Yang & Liao, 2007) a condition where the carbon nanomaterial supports remain stable without a thermal degradation or gasification.

For utilization in a steam reforming operation, the results from an experimental study by Tobias et al. (2006) with the objective to purify post-synthesized carbon nanotubes using steam at 1 atm water pressure can be used as an indication of the stability of the filamentous carbon in the presence of steam. The findings revealed that the purification by steam treatment at temperatures of up to 900 °C for 4 hours removed amorphous carbon and some of the graphitic particles (following reactions $C + H_2O \rightarrow CO + H_2$ and $CO + H_2O \rightarrow CO_2 + H_2$) entangling the SWCNTs, leaving behind only cleaner and steam-stable SWCNTs. The metal particles used to catalyse the SWCNTs growth were exposed due to the gasification of the nanotubes' end cap by the steam. The exposed metal particles were then removed by concentrated HCl. This demonstrates a potential of stable SWCNTs as the textural promoter for utilization in the steam reforming operation. Similar results were observed in the case of MWCNTs in a pure steam treatment at 900 °C but the purification took place in a shorter period, leaving behind cleaner, steam-stable MWCNTs for potential utilization in steam reforming.

Several studies employing carbon nanomaterials-based catalysts in gas phase reactions involving steam have been reported in the literature but the stability of the carbon nanomaterials was not reported at the end of each of the experiments; Ni/MWCNTs, Co/MWCNTs, Pt/MWCNTs and Rh/MWCNTs catalysts for steam ethanol reforming (Seelam et al., 2010), Cu-ZnO/MWCNTs for steam methanol reforming (H.-M. Yang & Liao, 2007), NiO/MWCNTs catalyst for steam propane reforming (López et al., 2012), Cu/MWCNTs catalyst for oxy-steam methanol reforming (Mierczynski et al., 2016), and Cu/CNFs catalyst for water gas shift (Oliveira et al., 2015). As far as we are concerned, there have not been any articles published in the literature that reported a demonstration of SWCNT-based catalyst in a reaction involving steam as one of the reactants in the gas phase. The highest operating temperature demonstrated thus far is the experimental study on steam reforming of propane

over MWCNT-supported nickel catalyst (López et al., 2012), where the reactions were run up to a maximum temperature of 800 °C.

However, the stability of the MWCNTs/CNFs in terms of chemical stability and/or thermal degradation was not made part of the above studies. Therefore, we are unable to analyse at which temperature point the carbon nanomaterials supports of the spent catalysts used in their respective work would have started to thermally deteriorate or been gasified. With the industrial SMR operation typically taking place between 500 and 950 °C (Mohammadzadeh & Zamaniyan, 2002; Zamaniyan et al., 2011), it is expected that the carbon nanomaterials would maintain good stability in the presence of steam in the SMR operation, but a thorough analysis of the condition of the catalysts in the reactions over reaction time must be performed to validate this. In addition, the duration of the reaction was not reported in any of the works above. All of the studies were performed at laboratory scale with the reactions over the same catalysts typically lasting only a few hours, and the catalysts were not operated in a continuous mode. Therefore, the stability of the carbon nanomaterials in the presence of steam at high temperatures for energy intensive reactions such as SMR may have not been satisfied by the existing studies reported in the literature.

4.3 Mechanical properties

The synthesis techniques to produce carbon nanomaterials have the capability to control the amount, thickness, and homogeneity of the coating on a monolith structure as a novel catalyst support material (J. K. Chinthaginjala & Lefferts, 2009; Morales-Torres et al., 2009). Growth of thin carbon nanomaterials (~12 nm) is faster and relatively straight, preventing their entanglement. On the other hand, the growth of thicker carbon nanomaterials (~35 nm) occurs at a lower rate, and in random and changing directions, which results in highly interweaving structures. This interweaving or entanglement has been found to be responsible for the formation of stronger aggregates. In addition, an increase in the growth time would increase the density of the carbon nanomaterial agglomerates, and subsequently contributes to further increase their mechanical strength (J. K. Chinthaginjala et al., 2007). The application of a layer of carbon nanomaterials as a catalyst support relies on its mechanical properties.

Based on various experimental works reported in the literature, Qian et al. (2002) summarized the tensile strength of CNTs in the range of 50 – 200 GPa. It was also reported that the entangled carbon nanomaterial clusters have a bulk crushing strength of 1 MPa (De Jong & Geus, 2000), making them attractive in fixed bed reactor applications. Satrio et al. (2005) developed a steam reforming methane catalyst for a laboratory-scale system in the form of small spherical pellets made of alumina and loaded with nickel particles. The average radial crushing strength in their work varies between 0.6 MPa (4.5 N/mm based on pellet diameter (pellet overall diameter = 4.5 mm)) and 1.3 MPa (9.9 N/mm based on pellet diameter (pellet overall diameter = 4.7 mm)). Redwan et al. (1990) developed the mechanical test methods using a Lorentzen & Werte (Stockholm, Sweden) Model 506 crush tester to determine the crushing strength of three different commercial SMR catalysts used in an industrial-scale operation. At least 25 catalyst pellets (to get a fair average of the crushing strength of one catalyst pellet) were crushed between a moving top plate and a stationary bottom plate, and the force at rupture was recorded automatically for each pellet. The measurements were performed according to ASTM D4179-82. The average radial crushing strength values were reported to be 1.0, 1.6 and 3.3 MPa each.

Based on the information above, it is believed that the entangled carbon nanomaterial clusters would mechanically survive in the SMR operation conditions. Nevertheless, there is another critical property that requires special attention. As discussed in our previous article (Baharudin & Watson, 2017b), one crucial criterion when selecting the monolithic substrate material for an application in the highly endothermic SMR operation is the CTE. It is recommended that the structure's substrate material of choice exhibits a comparable CTE with the reformer tube material so that the expansion and contraction of both the monolith and the reformer tube would take place at similar rates during operation, to avoid catalyst crushing. While a typical reformer tube made of IN519 exhibits a CTE of 17.1 x 10^{-6} K^{-1} (*INCO Databooks. IN-519 Cast Chromium-Nickel-Niobium Heat-Resisting Steel* 1976), the CTE of both SWCNTs and MWCNTs was reported to be negligible (Ma, Siddiqui, Marom, & Kim, 2010). Therefore, this is another factor that has been identified as a potential challenge that might hinder the application of carbon nanomaterials in SMR. However, the area of CNT attachment is extremely small, and (presumably) discrete. Therefore, the amount of stress generated on each individual CNT may not be very large, relative to the strength of the CNT. Nonetheless, an experimental validation to test the crushing strength of the carbon nanomaterials in the reformer

tube, by subjecting them to thermal cycles could be useful, as part of the qualifying exercises for their application in steam reforming.

D. Wu & Zhang (2013) discussed the applications of monolithic catalysts in the industry and concluded that more often than not the shutdowns for catalyst replacements were due to the mechanical failure, not the loss of catalytic activity. This makes the mechanical test a very crucial step in qualifying the employability of the monolithic catalysts. The mechanical test method has been mainly by ultrasonic means due to the convenience of the laboratory setup and quick measurement of weight loss of the catalytic washcoat layer from the ultrasonic vibration. The ultrasonic vibration and thermal shock tests to investigate the stability of the adhesion of washcoat layer made of γ-alumina on cordierite monoliths demonstrated by D. Wu & Zhang (2013) can be adopted to test the adherence of carbon nanomaterials on the metal monoliths. Other methods that can be adopted in the adhesion examination include exposing the monoliths in a hot air stream in a laboratory-scale tubular reactor with weight loss being measured as a function of time (Christos Agrafiotis & Tsetsekou, 2000a, 2000b; C Agrafiotis, Tsetsekou, & Ekonomakou, 1999), and a novel dual compression-tension technique by a mechanical testing system (Adegbite, 2012).

4.4 Thermal conductivity

Carbon nanostructures have a highly anisotropic thermal conductivity. For instance, at room temperature, the thermal conductivity of carbon nanotubes was found to be greater than 3000 W/(mK) (Han, 2005; P. Kim, Shi, Majumdar, & McEuen, 2001) along the filament axis, which is the a-axis (in-plane) of the graphene layer but only 1.52 W/(mK) (Sinha, Barjami, Iannacchione, Schwab, & Muench, 2005) along the c-axis (out of plane), which is along radial direction of a nanotube (Taha, Mojet, Lefferts, & van der Meer, 2016). This suggests that the structural arrangement of graphene layers influences significantly the thermal properties of the substrate material (Taha et al., 2016; Tuzovskaya et al., 2012).

There are three main structural arrangements of the graphene layer; the graphene sheets of perfect cylindrical arrangement (CNTs), conical arrangement (fishbone CNFs) and flat

arrangement (stacked CNFs). The parallel walls of the carbon nanotubes exhibit a greater thermal conductivity in the axial direction of the filament. This is attributed to the continuous straight graphene planes in the axial direction. The graphene sheets of the fishbone structures on the other hand are short and placed cross-wise to the axial direction, one on top of the other. The axial heat transfer is less efficient due to weak interlayer interactions between those short sheets. The fishbone structured arrays have thermal conductivity of 12 – 40 W/(mK) (Tuzovskaya et al., 2012).

Based on theoretical calculations and experimental measurements, it has been demonstrated by Han (2005) that carbon nanotubes have excellent thermal properties at room and elevated temperatures. An extremely high thermal conductivity due to the strong carbon-carbon bond of the graphene layers makes carbon nanotubes a novel material in the research of heat transfer improvement (Taha et al., 2016). Separate studies have been undertaken to measure the thermal conductivities of the single-walled (SWCNTs) and the multi-walled carbon nanotubes (MWCNTs) at different temperatures and the results have been compiled in a number of review papers. Based on the compilation of the thermal properties between the single-walled and the multi-walled carbon nanotubes (Teo, Singh, Chhowalla, & Milne, 2003) at room temperature, single-walled carbon nanotubes were demonstrated to possess a wide range of thermal conductivity values from 1750 to 5800 W/(mK), while all multi-walled carbon nanotubes exhibited a thermal conductivity of above 3000 W/(mK). Based on the information obtained from these findings, it is suggested that the multi-walled carbon nanotubes' structure should be the structure of choice for the application in highly energy intensive heterogeneous reactions in the context of our discussion, as their average thermal conductivity values are always greater than 3000 W/(mK).

However, the thermal properties of the carbon nanotubes also strongly depend on their quality, which is measured in the form of degree of crystallinity, shape and size of the crystallite, and presence of any impurities (Taha et al., 2016; Tuzovskaya et al., 2012). The thermal conductivity of a layer of carbon nanotubes can go down as low as 80 W/(mK) as a result of material imperfections such as structural defects, the presence of amorphous carbon, or the presence of impurities (Tuzovskaya et al., 2012).

In summary, CNTs are favoured in applications where effective heat transfer is desired, and MWCNTs which have a high degree of crystallinity and an absence of impurities have been identified to exhibit a very good thermal conductivity. However, this is not an ultimate conclusion as there has never been any comparison made in a single study on understanding the heat transfer characteristics in carbon nanofibers, single-walled carbon nanotubes, multi-walled carbon nanotubes and other carbonaceous materials such as graphene, graphene oxides and activated carbon, for a concrete finding to be established.

4.5 Surface chemistry properties

The graphene layered structure in carbon nanomaterials (Figure 3) has surfaces that can be divided into two kinds, namely basal plane and prismatic plane surfaces. The basal plane surfaces consist of only carbon atoms. These surfaces are homogeneous and "smooth", and therefore are ideal, and free of contaminants and defects. On the other hand, the prismatic surfaces have oxygen-containing groups other than carbon and are heterogeneous and "rough" (Olivier et al., 2001; Olivier & Winter, 2001).

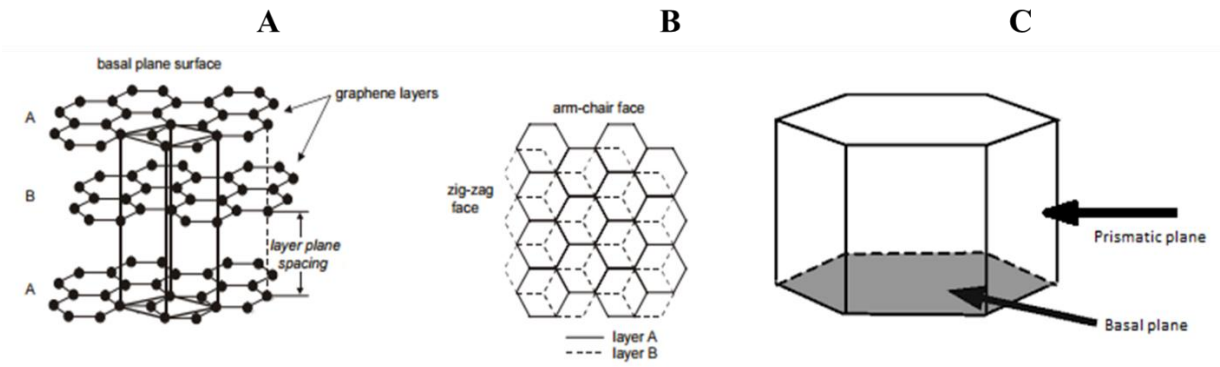

Figure 3: A) Schematic of AB hexagonal graphene layer stacking sequence and the unit cell (Olivier et al., 2001). Reproduced with permission from the author. Paper presented at the Proceedings of the ABA-2, International Conference on Advanced Batteries and Accumulators, Brno (Czech Republic).; B) Upright view of the basal plane of hexagonal graphite, where prismatic surfaces can be further subdivided into arm-chair and zig-zag faces (Olivier et al., 2001). Reproduced with permission from the author. Paper presented at the Proceedings of the ABA-2, International Conference on Advanced Batteries and Accumulators, Brno (Czech Republic).; C) 3-dimensional view of a unit of hexagonal graphene layers stack.

A good metal dispersion and stability is induced when the active metal particles are deposited on the prismatic graphene edges. The metal–carbon interaction is peculiar and varies with various carbon growth factors that determine the crystallinity of the grown carbon structure. Similarly, a controlled ratio between the prismatic edge and the basal plane is possible but it requires synthesis investigations and an in-depth analysis through selection of the various combined factors in the carbon nanomaterials' growth synthesis, which include the catalyst type and precursor, the carbon source, and the growth conditions (P. Li et al., 2006; Y. Li et al., 2006; J. R. Rostrup-Nielsen, 1972; Teo et al., 2003).

Typically, the as-synthesized (pristine) carbon nanomaterials contain carbonaceous impurities in the form of amorphous carbon sitting on the outer surface of the graphitic carbon. Metal impurities may also be present in the carbon nanomaterials synthesized by the catalytic techniques (Hou, Liu, & Cheng, 2008). The use of an etchant gas such as alcohol, ammonia or steam (Tobias, Shao, Salzmann, Huh, & Green, 2006; F. Yang et al., 2016) to remove the carbonaceous impurities *via* gasification has been a common practice as these disordered carbon are less stable than the highly crystallized graphitic carbon nanostructures. This is normally followed by removing the metal impurities (used to catalyse the growth of the carbon nanomaterials) by concentrated acid treatment (Hou et al., 2008). Such less stable carbon species can also be removed under steam-rich SMR conditions. However, an idea of removing them by the etchant gases treatment prior to their employment in the SMR reaction will leave behind only highly purified and highly ordered carbon nanomaterials that will survive under the SMR conditions without being gasified by the reactive gases.

The filamentous carbon offers the ability to modify the surface chemistry to suit as a catalyst support (Jitendra Kumar Chinthaginjala et al., 2010; J. K. Chinthaginjala & Lefferts, 2009), for an improved interaction between the carbon and the active metal particles that enhances the catalytic performance (Zhu et al., 2013). In addition, the large surface area of carbon nanotubes, both inside and outside, can be usefully exploited to support the reactant particles in catalytic conversion reactions (Teo et al., 2003). For this purpose, an interesting property of the carbon nanomaterials surface is its electrical property (J. K. Chinthaginjala et al., 2007; Teo et al., 2003). The sidewall surfaces of the carbon nanomaterials exhibit negative surface charge (Hamilton Jr et al., 2013) and these surfaces can further be functionalized using various

oxidative agents via techniques such as acid or basic treatment (Basahel, Al Thabaiti, Obaid, Mokhtar, & Salam, 2009; Datsyuk et al., 2008; Dreyer, Park, Bielawski, & Ruoff, 2010; Hamilton Jr et al., 2013; López et al., 2012; Moraes et al., 2011; Salmoria, Michelena, Barra, Vieira, & Paggi, 2013; Špitalský, Krontiras, Georga, & Galiotis, 2009; Stancu, Ruxanda, Ciuparu, & Dinescu, 2011; H.-M. Yang & Liao, 2007), polymer wrapping (Correa-Duarte & Liz-Marzán, 2006; Correa-Duarte, Pérez-Juste, Sánchez-Iglesias, Giersig, & Liz-Marzán, 2005; Correa-Duarte, Sobal, Liz-Marzán, & Giersig, 2004; Nam, Lee, Sim, & Choi, 2012; Nam, Souri, & Lee, 2016) and Hummers' method (J. Chen, Yao, Li, & Shi, 2013; Dimiev & Tour, 2014; Dreyer et al., 2010; Marcano et al., 2010), to introduce various oxygen functional groups (e.g. carboxyl, hydroxyl, carbonyl, etc.).

In general, carbon surface is hydrophobic in nature (Rodríguez-reinoso, 1998). The oxygen groups are able to alter the surface to a more negative charge that suppresses the hydrophobicity of the sidewall, in order to effectively adsorb the positive-charged cationic metal particles in aqueous solution for the catalyst synthesis. Therefore, the metal particles will be anchored and dispersed well on the surface of carbon nanomaterials. Although the oxygen-based functional groups may hypothetically not survive under the SMR conditions, in an oxygen-rich surface however, such oxygen groups will not be completely removed. Therefore, we hypothesize that the nickel catalyst for the SMR reaction would continue to have a strong interaction with the carbon nanomaterials support. However, we still need experimental evidence that demonstrates if CNTs would be advantageous to not allow the oxygenated groups to "creep" over the nickel nanoparticle's surface, blocking it at high temperatures.

Other than finding the importance of suppressing the hydrophobicity of the carbon nanomaterials surface for an effective catalyst synthesis, the functionalized surface also contributes to an enhanced catalytic reaction performance. A comparative study on the effect of hydrophobic (untreated) and hydrophilic (HNO_3-treated) surfaces of CNTs-supported catalysts on the catalytic performance of the hydrogenation of phenol by Xiang et al. (2014) revealed that the selectivity of producing cyclohexanone (more desirable product) over cyclohexanol (less desirable) was increased in the treated catalyst due to the surface hydrophilicity that preferentially adsorbed H_2O. This observation is of particular importance when designing the industrial catalysts used in the reactions that involve polar media such as

H_2O, which should also be able to be extended to reactions such as steam reforming and water-gas shift.

The effective removal of metal and carbonaceous impurities, as well as enhanced hydrophilicity or wettability of the graphitic carbon nanomaterials by measuring the concentration of the functional groups present in the treated carbon nanomaterials, as well as the zeta potential of their surfaces can be measured by various characterization tools. The characterization and analysis techniques include X-ray diffraction (XRD) or inductively coupled plasma mass spectrometry to measure the content of the metal impurities; Raman spectroscopy to measure the content of disordered and graphitic carbons in the samples; X-ray photoelectron spectroscopy and Fourier transform infrared (FTIR) spectrometer to measure and identify the presence of the various functional groups on the surface; and zeta potential to measure the negativity of the surface charge of the samples. The completion of the analyses is aided by morphology characterization using SEM and transmission electron microscopy to analyse the effect of functionalization on the crystallinity of the graphitic structure of the carbon nanomaterials, and TGA on the thermal stability. These characterization analyses and measurements on carbon nanomaterials pre- and post-functionalization using acid or basic treatment, polymer wrapping and Hummers' method mentioned earlier have been demonstrated in their respective work for further reference.

In the works investigating steam reforming reactions of various hydrocarbons and alcohols over various active metals supported on MWCNTs listed in Section 4.2, some of the authors reported the oxygen functional groups that were grafted on the surface of the acid-functionalized MWCNTs by presenting their Fourier transform infrared (FTIR) analysis, but some did not mention the specific oxygen groups obtained from their acid-functionalization work. Seelam et al. (2010) treated their MWCNTs with HNO_3 (70%) reflux for 13 hours and obtained carboxyl group (–COOH). Yang & Liao (2007) treated using HNO_3:H_2SO_4 (3:1) followed by dropping ethanol slowly into the solution and obtained carbonyl (–C=O) and hydroxyl (–OH) groups. López et al. (2012) treated using 3:1 ratio of H_2SO_4:HNO_3 at 80 °C for half an hour and obtained –COOH group. Mierczynski et al. (2016) did not report any MWCNTs pre-treatment technique and the oxygen groups in their work, while Oliveira et al. (2015) used HNO_3 (65%) but did not report the oxygen group obtained (although it is believed

to be –COOH as the functionalization work is similar to the one performed by Seelam et al. (2010)). On this basis, we are unable to make a judgement on the best oxygen groups for SMR, especially when the individual studies above were conducted on different steam reforming reactions under different conditions, using different active metals.

When the sidewall surface is grafted with the oxygen-moiety groups, the acidity level of the carbon nanomaterials increases and this introduces a potential coke deposition problem as the acidic surface promotes their capability to form coke. However, a lot of research initiatives in the catalyst synthesis stage that demonstrate a suppression of coke formation by controlling the nickel crystallite size (D. Chen et al., 2005; Guo et al., 2012; Y. Li et al., 2006) and doping the nickel with a second metal to create a basic (alkalized) surface (Trimm, 1999; Wu et al., 2013) can be considered for an adoption when synthesizing the catalyst in order to prevent the coke formation issue under the SMR conditions. This will be discussed in Section 6.

5. Challenges in employing carbon nanomaterials textural promoter in steam reforming

Coke formation is a common problem in steam reforming. It is however removable *via* coke gasification by increasing the steam to carbon ratio to above stoichiometric, but this option introduces a risk of parallel gasification of the carbon nanomaterials textural promoter on the metal monolith. This section deals with this issue where we will present our perspective based on sufficient literature evidence that under the same coke gasification conditions, the textural promoter in the form of high purity, highly crystallized carbon nanomaterials still maintains high stability and is not simultaneously gasified with the disordered, more reactive coke.

Balancing the coke formation and gasification at equilibria is also possible and an idea of making the carbon nanomaterials as a template for growing a conventional oxide support on the monolith structure would allow any risk of crystallized carbon support gasification to be completely eliminated. Other initiatives include research activities in optimization of the catalyst formulation during synthesis stage that creates unfavorable surface chemistry of the active metal-carbon interaction with respect to the formation of coke from the intermediates, and hence alleviating the coke formation in the first place.

5.1 Formation of carbonaceous materials in steam reforming operation

There are three mechanisms hot spots can occur as a result of coke deposition. Firstly, the pyrolytic carbon when deposited on the reformer tube's internal wall in a significant amount hinders the process gas flow and hence, creates hot spots due to uneven distribution of heat. Secondly, the hot spots occur due to encapsulation of the metal active sites by the coke deposits, leading to diminished catalytic performance, which in turn leads to the development of the hot-spot area as the externally supplied heat is no longer efficiently utilized by the reaction/process. This occurs when the metal active phase is surface-poisoned due to prevalence of metal carbide accumulation over gasification (see discussion of mechanism in Section 5.1.1.2). The carbides encapsulating the active surface are however removable and the catalyst activity can be regenerated by their gasification. If left untreated, such surface-only carbon atoms will form bulk coke deposits (amorphous or whisker coke). Thirdly, due to relatively higher mechanical strength of the whisker coke, fragmentation of the catalyst pellets would result when the growing whisker is forced into the catalyst supports' pore wall. Drift of the microscopic fragments of the catalyst pellets downstream can create plugs that will lead to pressure build-up in the reactor (Helveg, Sehested, & Rostrup-Nielsen, 2011; Trimm, 1997). Similar outcome could be envisaged in the case of formation of truly bulk amounts of coke that block the large pores of the extruded oxide support pellets eventually mechanically breaking the catalyst pellets into fragments. Either way, such inorganic oxide will form plugs which can NOT be gasified, irreversibly shutting down the reactor tube. This mechanism starves the zones below the coke-blocked pellets zone from the feedstock gas supply and in this way creates hot-spot zone there due to excessive externally supplied heat not being consumed by the reaction. At this stage the catalyst must be changed.

There are two ways the undesired coke deposition can occur in the steam reforming operation. Firstly, coke in the form of pyrolytic amorphous carbon is formed by non-catalytic decomposition of carbon-containing gas (thermal cracking/spontaneous-pyrolysis) at high temperatures (*ca.* 600 °C, depending on the types of carbon precursor); and secondly, coke in the form of whisker carbon is formed *via* catalytic cracking of the carbon-containing gas. The coke deposits in a reformer tube are present in the form of pyrolytic coke, whisker coke, and carbon nano-onion-like structures containing metal particles inside (Trimm, 1999).

It is therefore very crucial to understand the steam reforming conditions favouring the two ways of coke formation. Thermodynamically, coke formation under steam reforming reaction conditions is unfortunately unavoidable (Trimm, 1999). The pyrolytic coke deposition by both hydrocarbons cracking and CO disproportionation through spontaneous self-pyrolysis can take place at the high operating temperatures of steam reforming. In addition, nickel catalysts are vulnerable to deactivation by the catalytic formation of whisker carbon, even at a normal steam reforming operation conditions at which the high steam-hydrocarbon ratios ensure no thermodynamic affinity to form amorphous carbon deposits (Wu et al., 2013). The detailed mechanisms of catalytic whisker carbon formation over the nickel metal particles will be discussed later in order to understand it from the catalyst surface science point of view.

The catalyst deactivation by carbon poisoning is the subject of interest in our discussion in this section. Other mechanisms of catalyst activity loss include sulphur poisoning and catalyst sintering (J. Rostrup-Nielsen & Trimm, 1977; Trimm, 1997, 1999) especially in the presence of steam in the process gas. For example, the sintering phenomenon is well-known in the γ-alumina-supported nickel catalyst as the reaction proceeds over long period at high temperature, causing the loss of catalytically active phase surface area and hence activity loss (Moseley, Stephens, Stewart, & Wood, 1972). At a high operating temperature, the latter two causes of catalyst deactivation are equally crucial as the coke deposition, but they are not part of our discussion in this article.

In general, the reactions involved in a hydrocarbon steam reforming operation are (Trimm, 1997):

Overall reaction:

$$C_nH_{2n+2} + \frac{1}{2}(n-1)\,H_2O \rightarrow \frac{1}{4}(3n+1)\,CH_4 + \frac{1}{4}(n-1)\,CO_2 \qquad (9)$$

For paraffin:

$$C_nH_{2n+2} + n\,H_2O \rightarrow n\,CO + (2n+1)\,H_2 \qquad (10)$$

For methane (Bartholomew & Farrauto, 2006; Trimm, 1997):

$$CH_4 + H_2O \leftrightarrow CO + 3\,H_2 \qquad -\Delta H^0_{298} = -206\ \text{kJ/mol} \qquad (11)$$

For olefins (Bartholomew & Farrauto, 2006; J. R. Rostrup-Nielsen, 1974):

$C_nH_m + n\ H_2O \leftrightarrow n\ CO + \left(n + \frac{m}{2}\right)H_2$ $\quad -\Delta H^0_{298} = -1175$ kJ/mol (for n-C_7H_{16}) (12)

$CO + 3\ H_2 \leftrightarrow CH_4 + H_2O$ (13)

The water gas shift (WGS) reaction also takes place in the reforming operation.

WGS (Bartholomew & Farrauto, 2006; J. R. Rostrup-Nielsen, 1974; Trimm, 1997):

$CO + H_2O \leftrightarrow CO_2 + H_2$ $\quad -\Delta H^0_{298} = +41$ kJ/mol (14)

In the presence of steam, carbon monoxide, hydrogen, methane and/or other higher hydrocarbons (paraffins, olefins or aromatics), the reactions involved in the coke formation are possible through endothermic hydrocarbon dissociation and/or exothermic carbon monoxide dissociation (the Boudouard reaction) (Bartholomew & Farrauto, 2006; Helveg et al., 2011; J. R. Rostrup-Nielsen, 1972; Trimm, 1997, 1999; Wu et al., 2013):

$2\ CO \leftrightarrow C + CO_2$ (Boudouard Reaction) $\quad -\Delta H^0_{298} = +172.5$ kJ/mol (15)

$CH_4 \leftrightarrow C + 2\ H_2$ $\quad -\Delta H^0_{298} = -75$ kJ/mol (16)

$CO + H_2 \leftrightarrow C + H_2O$ (17)

$C_nH_{2n+2} \rightarrow n\ C + (n + 1)\ H_2$ $\quad -\Delta H^0_{298} = -188$ kJ/mol (for n-C_7H_{16}) (18)

5.1.1 Underlying mechanisms

5.1.1.1 Pyrolytic coke

In the absence of a catalyst, hydrocarbons and carbon monoxide decompose at elevated temperatures to form amorphous pyrolytic carbon. Moisala et al. (2003) presented the thermodynamics of the decomposition of carbon precursors in the form of Gibb's free energy change as a function of temperature (Figure 4).

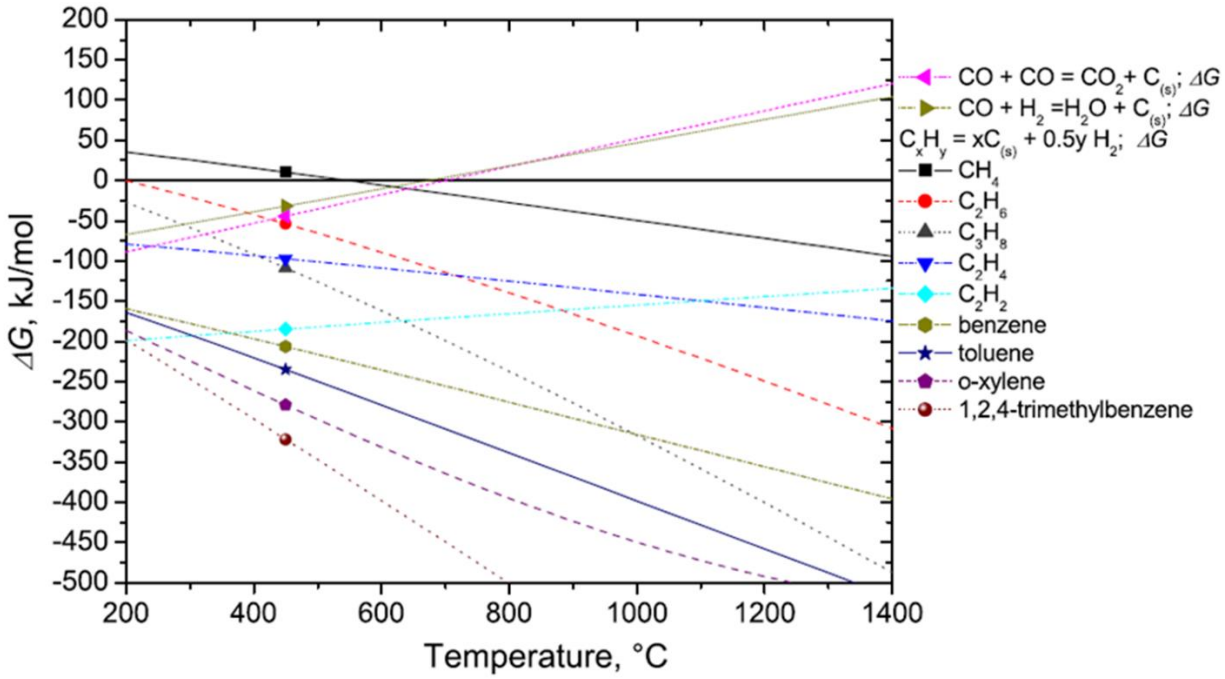

Figure 4: Thermodynamic data for self-pyrolysis of hydrocarbons and carbon monoxide (Moisala, Nasibulin, & Kauppinen, 2003). Reproduced with permission from IOP Publishing.

In general, an increase in carbon atom numbers per molecule in paraffinic hydrocarbons decreases the molecules' stability and hence, the thermal decomposition takes place at a lower temperature. The most stable hydrocarbon is methane and its thermal cracking begins at *ca.* 900 °C. For unsaturated hydrocarbons, the π-bonds in their structure are more easily activated making them more reactive with onset of their decomposition being as low as 200 °C based on thermodynamics calculation. However, at low temperature, the decomposition of the unsaturated hydrocarbons does not self-sustain without further energy input, and halts. At higher temperatures, however, their decomposition proceeds readily (Moisala et al., 2003). The complexity of the self-pyrolysis of the hydrocarbons emphasizes the importance of screening the gas composition and the concentration of the feed gas in the steam reformer to prevent an uncontrolled accumulation of amorphous coke deposits.

5.1.1.2 Whisker coke

Unlike pyrolytic coke that consists only from amorphous carbon at high temperatures, the whisker coke produced in the presence of a catalytic metal can have different degrees of graphitization from fully amorphous structures to highly ordered ones (R. T. K. Baker, 1989; Han, 2005; Peter J. F. Harris, 1999; Peter John Frederich Harris, 2009; Teo et al., 2003;

Wunderlich, 2006). The coke deposit's morphology has been identified and compiled, including but not limited to whisker coke deposits of disoriented or amorphous nature and well-graphitized structures closely related to the carbon nanomaterials, as well as various carbides (J. Rostrup-Nielsen & Trimm, 1977) and coke deposits adapted to the metal particle shape such as a pear-like shape with small metal fragments encapsulated inside (Helveg et al., 2011).

The ability of the metal catalysts to form the whisker is peculiar in that it varies with the chemical nature of the active metal catalyst and its precursor; the metal crystallite size; the carbon feedstock gas; and the conditions (chemical composition of the reactive gas atmosphere, temperature and pressure) of the whisker formation (J. K. Chinthaginjala et al., 2007; P. Li et al., 2006; Y. Li et al., 2006; J. R. Rostrup-Nielsen, 1972; Teo et al., 2003), which in turn affects the morphology and the degree of graphitization of the formed carbon structure can vary (J. K. Chinthaginjala et al., 2007; Helveg et al., 2011; J. Rostrup-Nielsen & Trimm, 1977; Trimm, 1999).

The peculiarity is believed to be associated with their catalytic activity in each step involved in the mechanism of the whisker carbon growth model. There are many carbon growth models postulated by researchers, with the one developed by R. Baker et al. (1972) being the most commonly agreed upon. The sequence starts when the carbon precursor gas dissociates on the exposed-side surface of the active metal particle; then the dissociated carbon dissolves in the metal particle; followed by the dissolved carbon diffuses through the particle; and finally the diffusing carbon precipitates at the other side of the metal particle's surface resulting in the growth of the carbon. The carbon precipitation eventually encapsulates the metal particles until they are no longer active (*i.e.* there is no clean metal surface available to continue decomposition of the feedstock gas) which stops further growth of the carbon. Similarly to the growth of carbon nanomaterials by CCVD on a monolithic structured substrate, the deposition of the coke can yield a tip- or a base-growth filament on the metal nanoparticles anchored onto porous support depending on the strength of the interaction between the catalytic active metal and the catalyst support (Geng et al., 2004). There are various other debatable versions of the growth model suggesting different mechanisms proposed by the research community and they have been reviewed by Teo et al. (2003), Chintaginjala et al. (2007), and Kock et al. (1985) for further reference.

The deactivated metal (when completely encapsulated) will become active again and the growth of the carbon may resume after regeneration of active metal particle surface by removal of encapsulating carbon *via* gasification by reactive gases such as oxygen, steam and/or hydrogen (Nazim Muradov, Smith, & Ali, 2005; J. R. Rostrup-Nielsen, 1972; Trimm, 1997, 1999; Zhang & Amiridis, 1998), which can be achieved under conditions of the steam reforming. The coking and decoking cycle continues but the phenomena could vary with changes in the composition of the reactive gases and the temperature. This will be discussed in further detail in Section 5.2.

As discussed by Moisala et al. (2003) in their review article, specifically for carbon monoxide disproportionation (eq. (15)) on the surface of a highly porous nickel at a normal pressure, the effective decomposition temperature is limited by kinetics and thermodynamics to a range of 520 – 800 °C, where the carbon dissolution through and precipitation from the metal particle may not be optimal. An increase in the CO pressure shifts the effective decomposition temperature to a higher range, as specified in Figure 5. This means that the higher the concentration of CO in the process gas, the less effective its decomposition becomes at a constant operating temperature. We are of the opinion that this phenomenon may be attributed to the decomposition of formed nickel carbide at the catalyst surface in this temperature range, which relates to prior studies back in the 1970s (J. R. Rostrup-Nielsen, 1972) and 1980s (De Bokx, Kock, Boellaard, Klop, & Geus, 1985; Kock, De Bokx, Boellaard, Klop, & Geus, 1985) described hereafter.

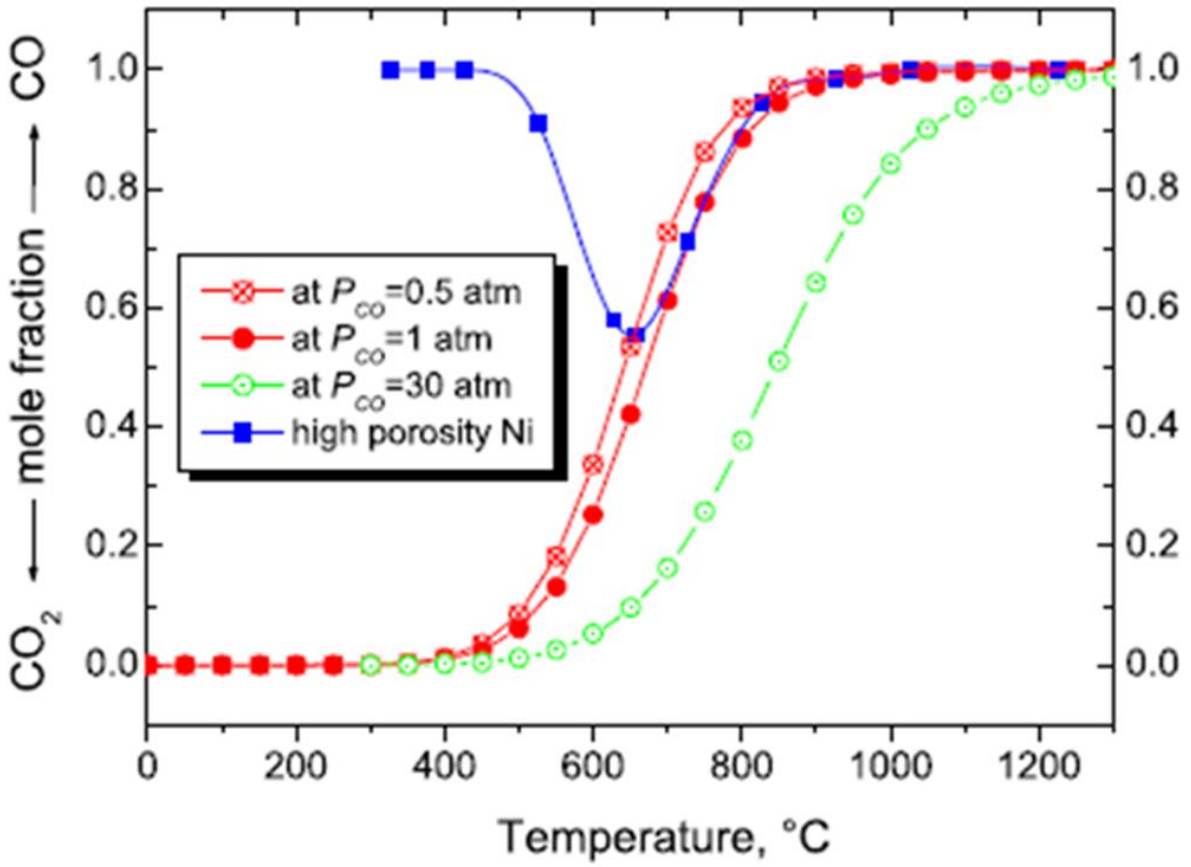

Figure 5: CO equilibrium concentration as a function of temperature at different pressures, and kinetic data for CO dissociation on a highly porous nickel (Moisala et al., 2003). Reproduced with permission from IOP Publishing.

De Bokx et al. (1985) and Kock et al. (1985) proved that the carbon dissolution into the nickel particle in the carbon growth mechanism model is preceded by a formation of sub-stoichiometric nickel carbide intermediate at the Ni catalyst surface following the proposed reaction equations of:

CO disproportionation (eq. (15)) on a Ni particle:

$$2\ CO + 3\ Ni \rightarrow Ni_3C + CO_2 \qquad (19)$$

CH_4 decomposition (eq. (16)) on a Ni particle:

$$CH_4 + 3\ Ni \rightarrow Ni_3C + 2\ H_2 \qquad (20)$$

The nickel carbide decomposes to carbon upon heating in the temperature range it becomes unstable; 400 to 1600 °C, followed by carbon dissolution into the nickel particle (J. R. Rostrup-Nielsen, 1972):

$$Ni_3C \rightarrow 3\ Ni + C \qquad (21)$$

Based on Figure 5, the CO disproportionation on the nickel is not effective between 520 and 800 °C due to the kinetics and thermodynamics limitation. The ineffectiveness could be explained by the decomposition of the nickel carbide that is taking place in this temperature range. Nonetheless, the carbide does not change the equilibrium constant of the CO decomposition reaction (J. R. Rostrup-Nielsen, 1972).

There have also been studies involving characterizing the metastable carbide intermediates formed on other metals, such as iron, reported in the literature (De Bokx et al., 1985; Kock et al., 1985; J. R. Rostrup-Nielsen, 1972). Indeed, in some cases, the mechanism of carbon nucleation over the metal particles did not even involve a metal carbide formation. These studies are not discussed in detail here as we are only interested in analysing the carbon formation specifically on nickel since it is used as a catalyst for the steam reforming reaction.

In principle, the surface of the various coke species formed in steam reforming could show some activity in further decomposition of methane, perpetuating the growth of such structures. This is evident by research initiatives (N1 Muradov, 2001; Nazim Muradov et al., 2005; Suelves, Pinilla, Lázaro, & Moliner, 2008) that investigated the catalytic decomposition of methane using carbonaceous materials of different structural and surface chemistry properties due to different morphologies and degrees of crystallinity that determine their structural and surface chemistry properties (*e.g.* activated carbon, carbon black, graphite, fullerenes, carbon nanotubes, diamond, *etc.*) as an active catalyst, without a presence of any active metals. The relevance of these investigations to our current context is the issue arising with the use of carbon materials as a textural promoter in the steam reforming reaction, which apparently could also be active for coke formation in the reforming environment.

Our analysis based on the outcomes of these studies (N1 Muradov, 2001; Nazim Muradov et al., 2005; Suelves et al., 2008) that were conducted at 850 – 900 °C indicates that the activity of the carbonaceous materials in methane decomposition follows a general trend of carbon-based materials' activity which decreases in the direction from the disordered form to well-graphitized, crystalline structures. This is evident by the kinetics curves of methane decomposition as a function of time over a range of carbonaceous materials tested by N1 Muradov (2001) and Nazim Muradov et al. (2005) as shown in Figure 6. Noteworthy, the

MWCNTs (Figure 6C) exhibited one of the lowest catalytic activities amongst the tested materials, with no increased activity during the initial period typical for other materials. Thus, pure MWCNTs with low catalytic activity in decomposition of methane are the carbon nanomaterials to act as a textural promoter on a metal monolith for steam reforming.

For a more detailed discussion on the activity behaviour of the carbonaceous materials in relation to their textural properties (*e.g.* surface area) and surface chemistry (*i.e.* the kinetics of the carbon-catalysed methane decomposition rate that varies with the apparent activation energy), reference can be made to the articles cited in this discussion (N1 Muradov, 2001; Nazim Muradov et al., 2005; Suelves et al., 2008). A half-order reaction kinetic equation has been proposed for the carbon-catalysed methane decomposition investigated over a range of carbon-based catalysts, giving the rate equation of (Nazim Muradov et al., 2005):

$$-r_{\mathrm{CH_4}} = \mathrm{k}P_{\mathrm{CH_4}}^{0.5} \qquad (22)$$

However, the studies that have been conducted so far have not managed to gather sufficient information on the intrinsic catalytic properties of the carbonaceous materials, for a well understood decomposition mechanism over the different carbon forms and the nature of the active sites accountable for the catalytic activity to be established (N1 Muradov, 2001).

Nazim Muradov et al. (2005) also extended their investigation to elucidate the effect of the surface oxygen group presence or absence on two samples of activated carbon; naturally oxygenated (*i.e.* containing some oxygen-based functional groups generated during fabrication of material) and deoxygenated (where such functional groups were chemically removed by treatment with pure hydrogen at 850 °C) respectively, and found that the carbons' catalytic activity could not be solely attributed to the oxygen-moiety groups, although these groups could have played a role in enhancing reactivity during the initial stage of the methane dissociation.

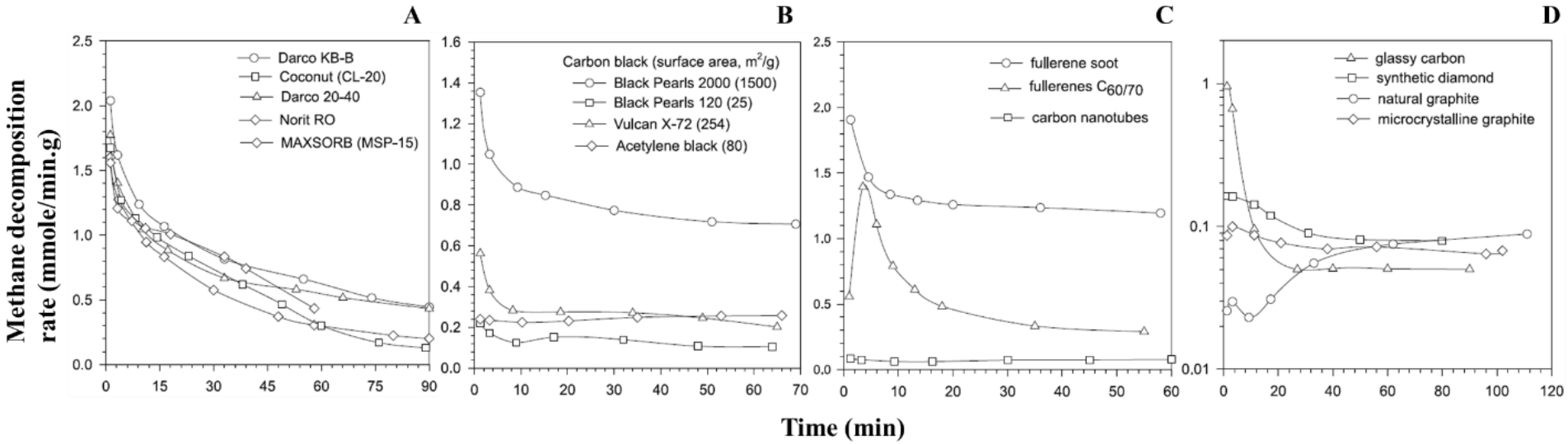

Figure 6: Methane decomposition over various carbonaceous materials: A) activated carbon; B) carbon black; C) nanostructured carbon; D) glassy carbon, synthetic diamond and graphite (N1 Muradov, 2001). Reproduced with permission from Elsevier.

5.1.2 Reaction conditions

CCVD is a catalytic decomposition of a carbon-containing gas, a method that offers flexibility to produce the carbon nanomaterials in the range of morphologies, from CNFs to CNTs in the forms of either MWCNTs or SWCNTs, by manipulating the chemical interaction between carbon and the catalyst metals. Hydrocarbon decomposition is also an upcoming popular reaction pathway in the production of the high purity hydrogen (Baharudin & Watson, 2017a). The reaction conditions in the "controlled" synthesis of carbon nanomaterials through CCVD by the carbon precursor's cracking in the presence of metal nanoparticle catalysts, typically cobalt, iron and nickel (J. K. Chinthaginjala et al., 2007; Moisala et al., 2003; Teo et al., 2003) needs to be understood first. They follow the same pathways and take place under somewhat similar conditions where the "uncontrolled" undesired coke is formed in the steam reforming operation through eq. (15), (16) and/or (18). The only critical difference between the "controlled" carbon nanomaterials' synthesis and the "uncontrolled" coke formation is that in the former, the hydrocarbons cracking and/or CO disproportion take place in the absence of steam, which is active for carbon gasification. However, there are exceptions to this critical difference when the "controlled" synthesis methods of the carbon nanomaterials use an etchant gas such as alcohol, ammonia or steam as a treatment to remove the disordered carbon. This is somewhat similar to the "uncontrolled" formation of coke under the reforming conditions where steam is present. This will be detailed further in Section 5.2 when we discuss the chemical stability of the different degrees of graphitization of the carbon nanostructures.

In a well-understood and "controlled" environment for carbon filament growth by a proper optimization of the growth factors discussed earlier, the formed carbon eventually deactivates the metal particles by encapsulation regardless of the morphology and crystallinity of the carbon nanostructure being formed. Therefore, it will be worthwhile to analyse under what conditions coke formation can occur when nickel is used as the active material supported on various inorganic oxides. The objective is to understand the conditions under which undesired coke deposition is not favourable in the presence of nickel-based catalysts in the steam reforming operating environment, which is more critical especially when nickel/multi-walled carbon nanotubes (Ni/MWCNTs) is used as the catalyst.

A temperature range of between 500 and 550 °C has been established as the range where the reaction (eq. (16)) is stable, but 550 °C is the most optimal as the reaction at any temperatures below this takes a longer time due to a slower decomposition of methane even though the carbon yield is the same, whereas an elevated temperature leads to an uncontrollable carbon growth leading to rapid catalyst deactivation.

Interestingly, the gasification of carbon on nickel catalysts (reverse of eq. (16)) also approaches its maximum at close to the same temperature; 552 °C reproducing the methane (De Bokx et al., 1985). The rate of the methane re-formation falls significantly with an increase in temperature and at 627 °C, the rate drops down to zero. The temperature of 550 °C is regarded as the optimal temperature based on the principles of atomic carbon accumulated on the active faces of the nickel surface responsible for the catalyst deactivation, which are then gasified to make these faces active again. At this temperature, based on the commonly accepted carbon growth mechanism model described earlier, the carbon formed by methane cracking at the nickel surface has not been dissolved into the nickel particle and is gasified at a maximum rate (Ermakova, Ermakov, & Kuvshinov, 2000). Zhang & Amiridis (1998) concluded that the catalyst eventually becomes deactivated due to coke deposition through blocking of the active sites or coke accumulation at the entrance of the particle pores that plug the access of the reactants to the particle's interior.

A small number of studies have been selected to be reviewed in this article based on their common findings. They were conducted with the objective of studying the production of hydrogen over various oxides-supported nickel catalysts at 550 °C by methane decomposition. Their findings can be useful in understanding the carbon (coke) yield in the context of our discussion.

Zhang & Amiridis (1998) observed slow deactivation of their silica-supported nickel-containing catalyst in the first 2 hours. This was followed by an accelerated loss of activity in the next hour, and the catalyst was deactivated completely in less than half an hour after that. An analysis of the spent and deactivated catalyst showed a carbon yield of 18 g/g Ni, which corresponds to a carbon accumulation of approximately 2700 carbon atoms per nickel atom,

based on the carbon amount calculated by methane conversion integration. It was said that only 10 carbon atoms are needed to block one active surface of a nickel atom. Ermakova et al. (1999) & (2000) conducted the study over nickel-containing catalysts supported on individual and mixes of two or three different oxides; Al_2O_3, ZrO_2, SiO_2 and MgO to study the contribution of different oxide supports. The reaction was stopped at the point where the hydrogen production reached 5% in the outlet gas concentration, but the duration taken to reach that point was not reported. The highest carbon yield of 375 g/g Ni for samples with an average NiO particle size of 22 – 36 nm was reported on SiO_2-supported catalyst, followed by Al_2O_3, ZrO_2 and MgO in the order of decreasing carbon yield. Mixes of support materials at different NiO particle diameters were also tested but not listed here.

Shaikhutdinov et al. (1997) in their work conducted two years earlier kept the same temperature of 550 °C in a methane decomposition reaction over nickel catalyst supported on CNFs, which showed a similar global catalytic performance as that over the alumina-supported catalyst, implying a common mechanism of carbon growth on the nickel surface regardless of the support. In addition to this, they also demonstrated the different outcomes of carbon yield and catalyst "life-time" based on different nickel precursors; chloride and nitrate. It was demonstrated that the chloride precursor gave a higher carbon yield of 245 g/g Ni but longer catalyst "life-time" of 17 hours before a complete deactivation, in comparison to 40 g/g Ni and 5 hours in the nitrate precursor. This also provides us with a piece of information that the "life-time" of the catalyst is longer before it gets to a complete deactivation when using CNFs as the support, compared to only slightly above 2 hours of the catalyst's "survival" in the study reported by Zhang & Amiridis (1998) using SiO_2 support.

5.2 Gasification of carbonaceous materials

In the environment where reactive gaseous components exist, the deactivated nickel particles encapsulated with the coke will become active again after its regeneration by carbon removal *via* gasification. In the steam reforming environment, the coke gasification follows the reverse of eq. (15) – (18) (J. R. Rostrup-Nielsen, 1972; Trimm, 1997, 1999; Zhang & Amiridis, 1998) in the presence of steam, hydrogen or carbon dioxide.

In addition, the removal of the undesired coke at the conditions where the reaction mechanisms are favouring gasification of the coke (*i.e.* decoking) is highly desirable by industrial operators in resolving the coke deposition issue. A couple of experimental works (R. Baker & Sherwood, 1981; Zhang & Amiridis, 1998) conducted to study the conditions for the gasification of the carbon on nickel surface in the presence of hydrogen and steam, are reviewed here. The catalyst regeneration can also be done by air oxidation following carbon combustion ($C + O_2 \leftrightarrow CO_2$) (Zhang & Amiridis, 1998), but this is not part of our discussion as we are analyzing only the decoking pathways in a typical steam reforming environment, where free diatomic oxygen is not present.

R. Baker & Sherwood (1981) reported the gasification of graphite deposited on nickel particles in the presence of steam, hydrogen, and steam–hydrogen flow. In brief, the gasification took place at above 900 °C in the presence of pure steam, 845 °C in dry hydrogen and 780 °C in wet hydrogen with a ratio of H_2/H_2O = 40:1. Zhang & Amiridis (1998) on the other hand investigated the gasification of carbon by steam to regenerate a completely deactivated nickel catalyst at a fixed temperature of 550 °C and observed a full restoration of the catalyst activity as evident by the formation of carbon monoxide and methane.

Typically, a ratio higher than the stoichiometric of the steam to carbon (in the hydrocarbon feed) ratio, S:C in the feed gas can also be applied in an attempt to halt the coke formation through the reverse of eq. (15) – (18), but this comes with a price of significant energy waste to generate more steam (Guo et al., 2012). On the other hand, the decoking of the formed coke *via* gasification would risk the gasification of the carbon nanomaterials support under the same conditions, when using this material as the textural promoter in the steam reforming reaction. The removal of the support causes activity loss of the catalyst due to sintering of the nickel particles.

There is also a rhetorical question of whether the active metal particles used to grow the carbon nanomaterials textural promoter in the CCVD process that get encapsulated in the grown carbon structure could be active in growing coke. Based on the discussion earlier, these metal particles are completely deactivated when encapsulated by the grown filamentous carbon. However, when being used in steam reforming where the reactive gases are present, the carbon

filament end-caps (and perhaps the graphitic wall of the carbon nanomaterials too) have a tendency to get removed *via* gasification. If this happened, we foresee two possibilities here:

(i) The loss of carbon nanomaterials support would cause the nickel particles meant for the steam reforming to sinter with each other, and with the previously encapsulated metal particles (used to grow the carbon nanomaterials), and hence, poison the steam reforming catalyst. The examination by Y. Li et al. (2006) who tracked the evolution of nickel particles during methane decomposition might be useful to support the speculation of this possibility. Based on their findings, the formed carbon changed the crystalline size and the morphology of the nickel particles. The nickel particles evolved from a fibrous structure to bigger-size particles due to sintering, which were then dispersed on the in situ formed carbon, resulting in pear-like shaped nickel particles.

(ii) The now exposed metal particles would be active to re-grow (undesired) carbon of random morphologies and crystallinities and completely deactivate the catalyst.

As far as existing literature is concerned, the closest work to address the change in surface properties of the nickel catalyst before and after the reaction is the study by López et al. (2012) in steam propane reforming using Ni/MWCNTs. Unfortunately, they only reported the characterization analysis of their synthesized catalysts of varied Ni loading content but did not do that on the spent catalysts post reaction tests.

As we are well informed, the as-synthesized CNTs by CCVD typically contain impurities in the form of: (1) the metal particles used to catalyse their growth are encapsulated by the carbon layers and capped at the end of the nanotubes; and (2) carbonaceous materials that include amorphous carbon, fullerenes, and carbon nanoparticles. The carbonaceous impurities are generally less stable in comparison to the highly crystallized graphitic carbon nanostructures in the conditions where reactive gas(es) is/are present, while the metal impurities are normally removed by concentrated acid treatment after the more reactive (less stable) carbonaceous impurities are removed (by gasification) from the as-synthesized CNTs (Hou et al., 2008).

Presented below is the work reported in the literature that demonstrated the purification of the as-synthesized CNTs by using steam to remove the impurities at temperatures comparable to the operating conditions of the steam reforming, that serve as evidences that high purity CNTs left behind post the steam treatment are highly stable. Therefore, we are convinced that they

can survive in the steam reforming conditions when being used as the textural promoter without being gasified in parallel with the gasification of the disordered carbon coke deposit. With these evidences, both the possibilities of (i) and (ii) described above do not arise after the as-synthesized CNTs are purified with steam treatment and concentrated acid since the less stable carbonaceous impurities and metal impurities are removed respectively, prior to depositing the active nickel nanoparticles for the purpose of catalysing the steam reforming reaction.

The work by Tobias et al. (2006) revealed that there was no evolution of gas (formation of CO and H_2 from the gasification of carbon by steam based on eq. (17)) when their as-synthesized single-walled carbon nanotubes (SWCNTs) were treated with pure steam at 750 °C for 2 hours. Only when the treatment temperature was raised to 900 °C, the reactivity of the amorphous carbon with the steam was observed, where there was no amorphous carbon after 2 hours of treatment seen on the high resolution transmission electron microscopic (HRTEM) image. At the end of 4 hours of steam treatment, cleaner SWCNTs were clearly observed on the HRTEM image, with no presence of the amorphous carbon and graphitic carbon particles entangling the as-synthesized SWCNTs that was seen prior to the treatment. In addition, the ends of the SWCNTs were also removed, revealing clearly the metal particles that were encapsulated earlier on, which was then removed by concentrated HCl. As-synthesized MWCNTs on the other hand showed an even shorter time to remove the impurities by steaming at 900 °C. This work provides a strong support and basis for the employment of CNTs as a textural promoter in steam reforming operation, where they are sufficiently stable (low reactivity) in the reaction conditions. A relatively recent study by F. Yang et al. (2016) introduced steps to synthesize highly purified SWCNTs that included steam treatment at 550 °C during the synthesis process, resulting in a final SWCNTs purity of 99.8% that presented an advantage of uniform band structure for high-end applications, which can be adopted when growing the CNTs on the monolithic structure as the textural promoter for the catalytic application discussed in our article.

Other than purification, steam is also used as an etchant to create higher specific surface area (SSA) and specific pore volume (SPV) of CNTs for various applications. The work by Xiao et al. (2014) demonstrated that steam etching of SWCNTs at 750 – 950 °C showed increasing values of both SSA and SPV of the SWCNTs as the treatment temperature increased, which introduced a novelty in the technique of synthesizing porous carbon nanotubes for making high

rate, large capacity lithium-sulphur batteries demonstrated in their work. This knowledge is also useful when synthesizing the CNTs for an application as a textural promoter in the catalysis application, since the above mentioned textural properties are useful for an effective diffusion of the reactant and product to and from the catalytic active sites. More importantly, based on XRD data, the steam etching in the work by Xiao et al. (2014) showed a large reservation of the intrinsic structure of the SWCNTs with only a small amount of damage, which could be deterioration of the amorphous carbon and the less stable carbonaceous impurities as in the case of the work by Tobias et al. (2006).

Another work on the etching of CNTs by steam was demonstrated at a lower temperature; Xia et al. (2007) conducted it at 600 °C, a slightly lower temperature than Xiao et al. (2014) but in the presence of iron nanoparticles that were impregnated on the surface of the originally non-etched MWCNTs. After the removal of the iron particles by acid treatment, the final result was MWCNTs of stable etched-tubular structure. The schematic of the steam etching of the MWCNTs by Xia et al. (2007) is shown in Figure 7. A successful steam etching work for synthesizing a porous graphene oxide network for a chemical sensing application performed by T. H. Han et al. (2011) at a very low temperature of 200 °C serves as an indication that graphene oxide is a lot less stable than CNTs (which require temperatures of as high as 750 – 900 °C to etch), supporting our perspective that CNTs can be the carbon nanomaterials that will survive steam reforming conditions without the risk of gasification when being employed as a textural promoter.

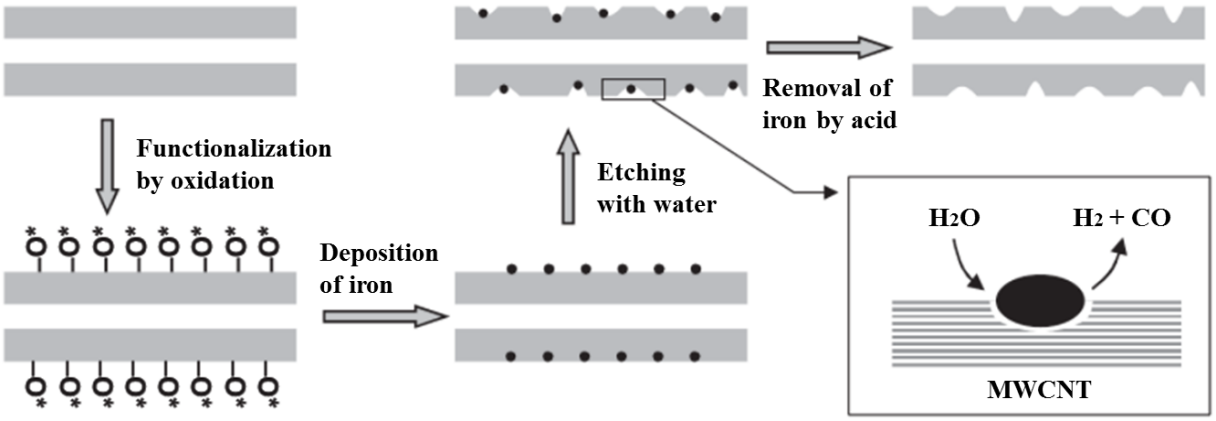

Figure 7: Schematic of steam etching of MWCNTs in the presence of iron particles (Xia et al., 2007). Copyright Wiley-VCH Verlag GmbH & Co. KGaA. Reproduced with permission.

6. Strategies to balance carbon formation and gasification in steam reforming operation

Even though it is highly likely that highly purified CNTs will survive steam reforming conditions without simultaneously being gasified together with the disordered carbon coke deposit, it is still best to avoid the coke formation in the first place. A number of initiatives have been taken in the research activities of catalyst synthesis and formulation and establishing operating guidelines to avoid coke formation in the steam reforming operation.

6.1 Development of steam reforming operating guidelines

A comprehensive operating procedure needs to be developed and strictly adhered to by the plant operators when using carbon nanomaterials in a steam reformer, to prevent coke in the first place so that there will be no issue with the carbon nanomaterials getting removed together with the coke at the points where carbon gasification is favoured. Coke formation, be it pyrolytic or whisker, can be minimized or inhibited by operating the reforming reaction at an optimal condition, balancing the coke formation and the gasification at equilibria (Helveg et al., 2011; Trimm, 1999).

It is generally agreed that the steam reforming proceeds *via* structure-sensitive dissociative adsorption of the hydrocarbons on the surface of the active nickel particle, where the activation energy on Ni (1 1 0) and Ni (1 1 1) is higher than that on Ni (1 0 0) (Beebe Jr, Goodman, Kay, & Yates Jr, 1987). The dissociation produces molecular hydrogen, while the remaining carbon in the hydrocarbons reacts with water to form more molecular hydrogen and carbon monoxide (Bengaard et al., 2002), in which for methane is written as (Trimm, 1999):

$$CH_4 + * = CH_x - * + \frac{(4-x)}{2} H_2 \quad (23)$$

$$CH_x - * = C - * + \frac{x}{2} H_2 \quad (24)$$

$$H_2O + * = O - * + H_2 \quad (25)$$

$$C - * + O - * = CO + 2* \quad (26)$$

A reasonable agreement between methane decomposition rate and the overall steam reforming rate infers eq. (23) as the rate determining reaction, where coke formation is slow (Trimm, 1999).

On the nickel surface, the hydrocarbons are dissociated into reactive monoatomic carbon species C_α that are easily gasified. In an excess C_α formation or slow gasification, some of the species get polymerized/rearranged to a less active C_β species, which may accumulate on the nickel particle surface or dissolve in it. The deposits on the surface that encapsulate and deactivate the catalyst are harder to gasify than the reactive C_α. Therefore, finding a balance between the rate of coke formation and the rate of coke gasification is crucial (Trimm, 1997, 1999).

A complete study on optimizing the operating condition in steam reforming of hydrocarbons in the early 1970s by Moseley et al. (1972) established the fundamental knowledge on the operating parameters that play the role in coke minimization in a series of experiments at a low temperature range of 450 – 500 °C through manipulation of space velocity, pressure, temperature and steam to carbon ratio (S:C) (C = carbon content in the hydrocarbons, not a free carbon). As a brief conclusion, the findings revealed that the coke formation: (i) is independent of the partial pressure of the hydrocarbons; (ii) increases with increasing feed rate and temperature; and (iii) decreases with the increase of S:C. If operated at an excessive temperature, the sintering effect is more likely causing a loss of active surface that leads to coke deposition by the Boudouard equilibrium and/or pyrolysis.

Thermodynamically, the conditions where the coke formation are favored in a nickel-catalyzed SMR can be quantitatively determined from the equilibria of eq. (15) or (16); SMR (eq. (11)); and WGSR (eq. (14)) (Bartholomew & Farrauto, 2006). A reference based on carbon limit diagrams that relates the propensity of coke deposition with the ratios of S:C and carbon dioxide:carbon presented by J. Rostrup-Nielsen (1993) can be used to perform data calculations to develop an operating guideline to determine an optimal condition in the steam reforming where the aforementioned four reactions are at equilibria (Trimm, 1997, 1999). Further reference can also be made to Bartholomew & Farrauto (2006) who developed a detailed modelling procedure to determine the carbon formation threshold as a function of specific

location of the catalyst pellet with respect to the distance in axial and radial directions of the reformer tube, guiding towards a selection of sufficiently high S:C that prevents carbon formation in any section of the catalyst bed in the reformer tube. In summary, the above examples show that it is possible to predict effects of S:C ratio on formation of coke taking reactor design into account.

6.2 Feedstock screening

When the feedstock gas contains higher hydrocarbons (HHC) (*i.e.* heavier feedstocks; higher molecular weight, boiling points) or unsaturated hydrocarbons, the effect of S:C is less effective in gasifying the coke. Relative to methane, the dissociative adsorption of the HHC on the nickel particle surface is a lot faster (eq. (23)), increasing the rate of the carbonaceous intermediate formation (eq. (24)). Hence, the carbon accumulation rate on the particle surface would also be faster, making the coking more pronounced (Trimm, 1999).

In addition to the HHC, the outcome from a series of experiments at a fixed S:C ratio to determine the coking rate in the presence of different types of hydrocarbons indicated a strong dependent on their unsaturated character (J. R. Rostrup-Nielsen, 1974). In general, the tendency for coke formation increases as the unsaturation and aromaticity in the feedstock gas increases (J. K. Chinthaginjala et al., 2007; Trimm, 1997).

A screening of the feedstock to not allow the gas with constituents prone to coke formation would indeed help to alleviate this issue in the steam reforming operation. In industrial practice, an adiabatic bed pre-reformer is used at the upstream of the tubular steam reformer to convert all the HHC and unsaturated hydrocarbons into an exit gas containing hydrogen, carbon monoxide, carbon dioxide and methane prior to feeding into the steam reformer. This also allows flexibility in processing various types of hydrocarbons feedstock.

6.3 Catalyst synthesis research

When it comes to specific studies aiming at minimizing the coke deposition, the metal–carbon interface has become the subject of interest in an attempt to understand the metal–carbon

interaction from a surface chemistry point of view, in such a way that the interaction can be distorted to bring down the rate of carbon formation. A brief review by J. R. Rostrup-Nielsen (1972) on the studies performed in the 1940s – 1960s provides evidence of a strong influence of crystal orientation in the surface chemistry of the carbon formation by CO disproportionation on monocrystalline nickel at 550 °C. Carbon was detected on the Ni (1 1 1) faces, but not found on the Ni (1 0 0) and Ni (1 1 0).

Transition metals such as copper and nickel are classified into the *d*-block metals. The transitional metal complexes have characteristic colours as a result of the absorption of light in the visible part of the spectrum. This is a result of an electron excitation by the light from a level occupied in a molecular orbital of the metal complex, to an empty level (T. Saito, 2004). The electronic properties of a catalyst are correlated by the percentage of the *d*-character of the catalyst. In ethene hydrogenation for instance, the catalytic activity of a nickel catalyst decreases with the number of *d*-band holes, when nickel is alloyed with copper (Davis, 2008). This is not the case in the coke formation reaction where the importance of the properties of the individual surface atom and its neighbours are more significant than the bulk phase electronic properties. This was supported by a study on the influence of the *d*-character of the metal using a copper-nickel alloy where the carbon formation selectivity turned out to still be favoured on the Ni (1 1 1) faces, as presented in Nielsen's review (J. R. Rostrup-Nielsen, 1972).

We have seen earlier in Section 6.1 that the dissociative adsorption of the hydrocarbons in the steam reforming reaction on the surface of the active nickel particle shows high activation energy on Ni (1 1 0) and Ni (1 1 1) (Beebe Jr et al., 1987). This indicates that the Ni (1 1 1) is the active face where the two reactions; steam hydrocarbons reforming and hydrocarbons/CO decomposition "compete". A comprehensive fundamental study of the surface chemistry of the nickel crystalline active sites and their interaction with the carbon-containing gases for both steam reforming and carbon formation was presented by Bengaard et al. (2002) for further reference. The analysis was based on density functional theory calculations, experimental kinetic investigations, micro-kinetic simulations, and relevant experimental data from the literature.

Whilst a number of studies reported success stories of enhanced catalytic activity through modified steam reforming catalysts in the form of nickel/nickel oxide deposited on different oxygenated carriers (*e.g.* alumina, zirconia, titania, silica, magnesia or a mix of two or more of them) (Kho, Scott, & Amal, 2016; T. W. Kim et al., 2015; Matsumura & Nakamori, 2004); relative activity ranking of various other noble and transition metals (Jones et al., 2008); and introduction of the second metal to the primary nickel (Wu et al., 2013), we are not making quantitative analysis as to how one catalyst is superior over the other in terms of reaction performance and/or energy efficient operation at lower operating temperatures. We will specifically discuss the associated problems in steam reforming operating conditions with regards to carbon laydown and indeed, we will limit our discussion to nickel-based catalysts only. Some of the reported works (Kho et al., 2016; Matsumura & Nakamori, 2004; Wu et al., 2013), whilst exhibiting success in bringing down the operating temperature of the reforming process (which subsequently leads to energy savings), can at the same time be a solution to prevent the pyrolytic coke formation favourable at high temperatures.

6.3.1 Nickel particle size

An earlier study in the 1970s by Moseley et al. (1972) revealed that the rate determining step in the hydrocarbons steam reforming reaction (*i.e.* eq. (23) – (26)) is dependent on the nickel crystallite size, which explains the different activity rate in the "competition" between the simultaneous steam reforming and hydrocarbons decomposition. When the nickel particles are finely divided, the steam reforming reaction is a chemically-controlled reaction in zeroth order with respect to the hydrocarbon and steam. The reaction order increases with the increase in the nickel particle size, and additionally, the activation energy for the overall reaction decreases. Therefore, the steam reforming becomes rate limiting as it is controlled by the slower gas diffusion in the pores of the larger nickel particle, suppressing the hydrocarbon/CO decomposition reaction. This study shows promising improvement on the resistance to coke deposition when nickel particles of a larger size are used, at a constant operating temperature and S:C ratio.

In a more recent study (D. Chen et al., 2005), it was demonstrated that too small of a nickel particle did not provide sufficient activity for the nickel to allow carbon formation (*i.e.* CNFs in this particular study), while too large of a particle was inactive due to too sluggish of a carbon diffusion through it. The trend for an optimal NiO crystallite size that favours CNFs yield at 580 °C developed in the study by Chen et al. (2005) is presented in Figure 8.

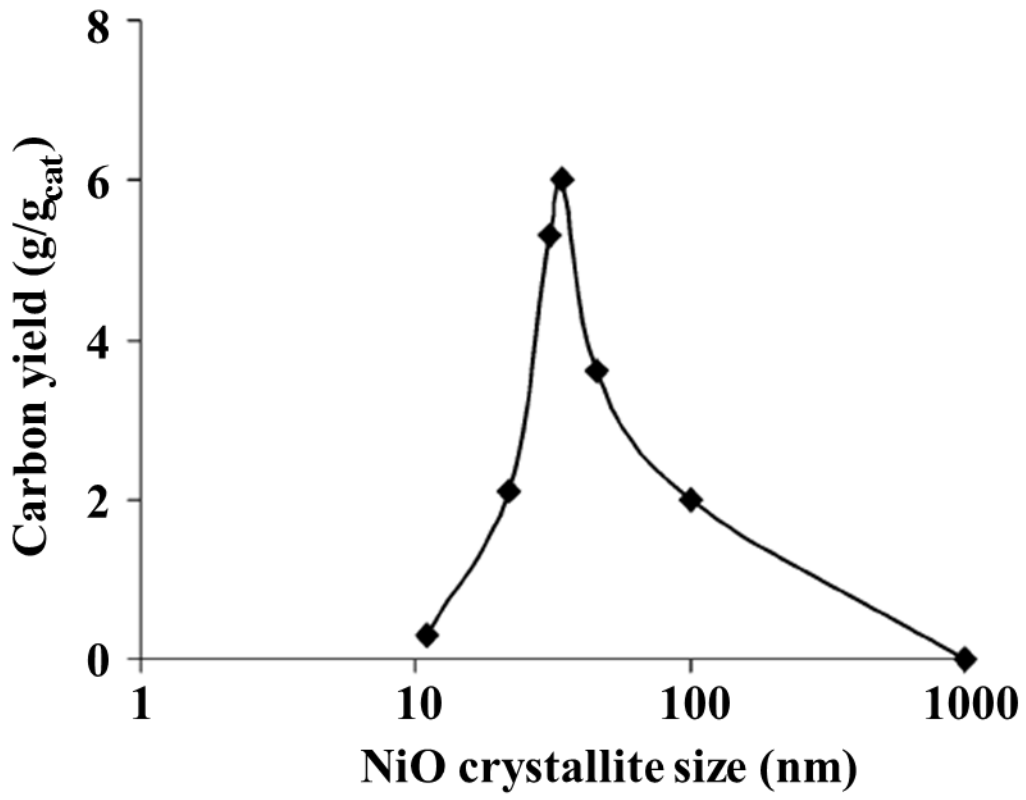

Figure 8: Carbon yield by CH_4 decomposition at 580 °C as a function of NiO crystallite size in the work by Chen et al. (2005). Reproduced with permission from Elsevier.

Based on the findings in a study of hydrogen production by methane decomposition at 500 °C conducted by Y. Li et al. (2006), they varied the nickel crystallite size *via* manipulation of the calcination temperature and showed the highest carbon (in the form of CNFs) and hydrogen yields at a crystallite diameter of 10.8 nm, while the size of 20 nm gave a reduction in the carbon yield, and the activity decreased down to a complete catalyst deactivation at 26 nm.

In the most recent study reviewed in this article, Guo et al. (2012) attempted a synthesis of the catalyst with an "optimal" size of nickel particle at the size of 14 nm that balanced the rate of

carbon formation and gasification in steam methane reforming reaction by employing a plasma decomposition of nickel nitrate aqueous solution using dielectric barrier discharge for the nickel particles deposition on SiO_2 support. Their technique was successful in producing uniformly crystallized particles and introduced a higher activation energy for methane decomposition on the highly coordinated sites of Ni (1 1 1), which led to a balanced carbon formation and gasification at low S:C ratios, but at the expense of a lower methane conversion.

6.3.2 Basic catalyst support

Even when operating at a S:C ratio favouring the gasification, its kinetics are slow since most of the time the process is only concerning the gasification of C_β that is less reactive than C_α. The gasification can be predominated by C_α if the polymerization/rearrangement of this species to C_β can be minimized (Figure 9) (Bartholomew, 1982; Trimm, 1997). The industrial catalyst formulation typically includes the use of alkali or alkali-containing oxide supports such as MgO and CaO to accelerate the carbon gasification (Trimm, 1997). Additionally, the acidity in the oxide supports of the nickel-based catalyst introduces acidic sites that can promote the activity of hydrocarbons cracking at the nickel particle surface (Baharudin & Watson, 2017a). Therefore, the addition of the basic metal oxides such as rare earth oxides has also been used to neutralize the acidic sites (Bengaard et al., 2002; J. R. Rostrup-Nielsen, 1974; Trimm, 1999).

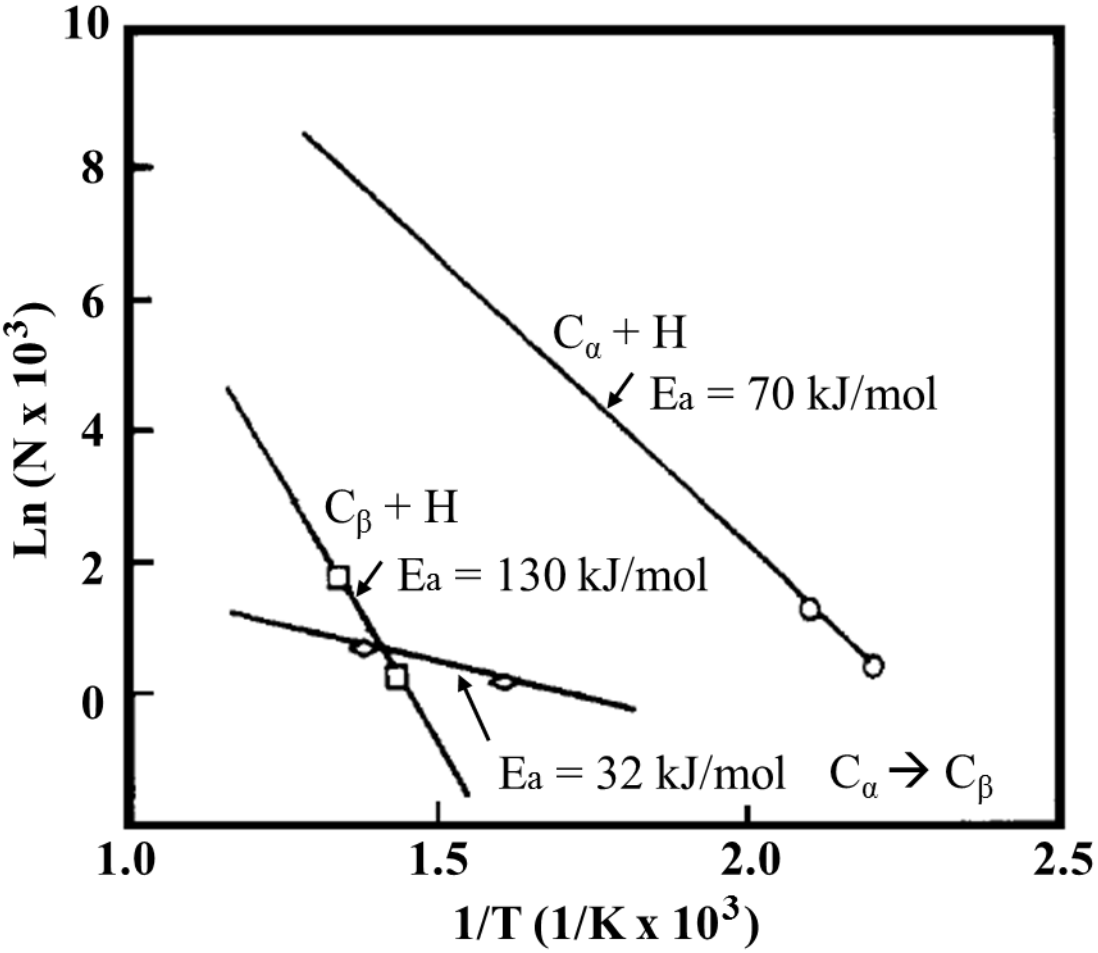

Figure 9: C_α and C_β gasification by hydrogenation and their inter-conversion (Bartholomew, 1982; Trimm, 1997). Reproduced with permission from Elsevier.

However, since the alkalized sites work to minimize the coke formation in such a way that the carbon gasification is accelerated, this is not quite the case when the support is made of the carbon nanomaterials such as in our proposal. Therefore, when using carbon nanomaterials as the support, it is crucial to wash off excess of the acids used during functionalization following the acid functionalization step that is needed to introduce oxygen-moiety groups on the sidewall surface by washing the functionalized carbon nanomaterials with water in abundance.

6.3.3 Metal dopant

Trimm (1999) reviewed the effect of dopants on the nickel catalysts while studying a bimetallic dopant–Ni catalyst system that showed favoured steam reforming with minimal coke deposition. H. Wu et al. (2013) reviewed a list of various second metals added to the primary

nickel for steam reforming, and the metals screened to have been able to suppress the coke formation when added in small amounts to nickel were Mo, Fe, B, Cu and Au. Of all the qualified screened metals, gold was found to be the only dopant capable to completely halt coke formation, under typical industrial steam methane reforming operation conditions. Adding Au serves as a potential solution when synthesizing the nickel catalyst supported on carbon nanomaterials as the textural promoter, as carbon support gasification can be avoided with the coke formation being prevented in the first place.

7. Prospect

The amount of active metal catalyst particle loading inventories deposited on the walls of monoliths of a given volume is less than the corresponding volume of a packed bed of small pellets (Giroux et al., 2005). Through the use of washcoating materials of high specific surface area, a comparable loading content is made possible by dispersing the active component on the washcoat layer and in its pores. Additionally, a more superior overall heat transfer coefficient in the monolithic support system improves the radial heat conduction that results in an enhanced SMR reaction performance, as evident by a couple of experimental demonstrations by Ryu et al. (2007) and Basile et al. (2008), which will be presented next. When carbon nanomaterials are used as a textural promoter on a monolith structure, their even higher specific surface area per unit volume enhances the interaction of the reactants with the active catalytic component deposited on them. Furthermore, the high thermal conductivity of the carbon nanomaterials itself helps to further enhance the heat transfer across the monolith structure, and subsequently improves further the conversion of methane.

Based on the discussion we have made thus far, the proposed concept of the structured catalyst system for the steam reforming application is graphically summarized and presented in Figure 10 for further discussion on its employment prospect in the reaction operation conditions. An illustration of a monolithic catalytic structure in reformer tube as proposed by Zamaniyan et al. (2010) is also shown.

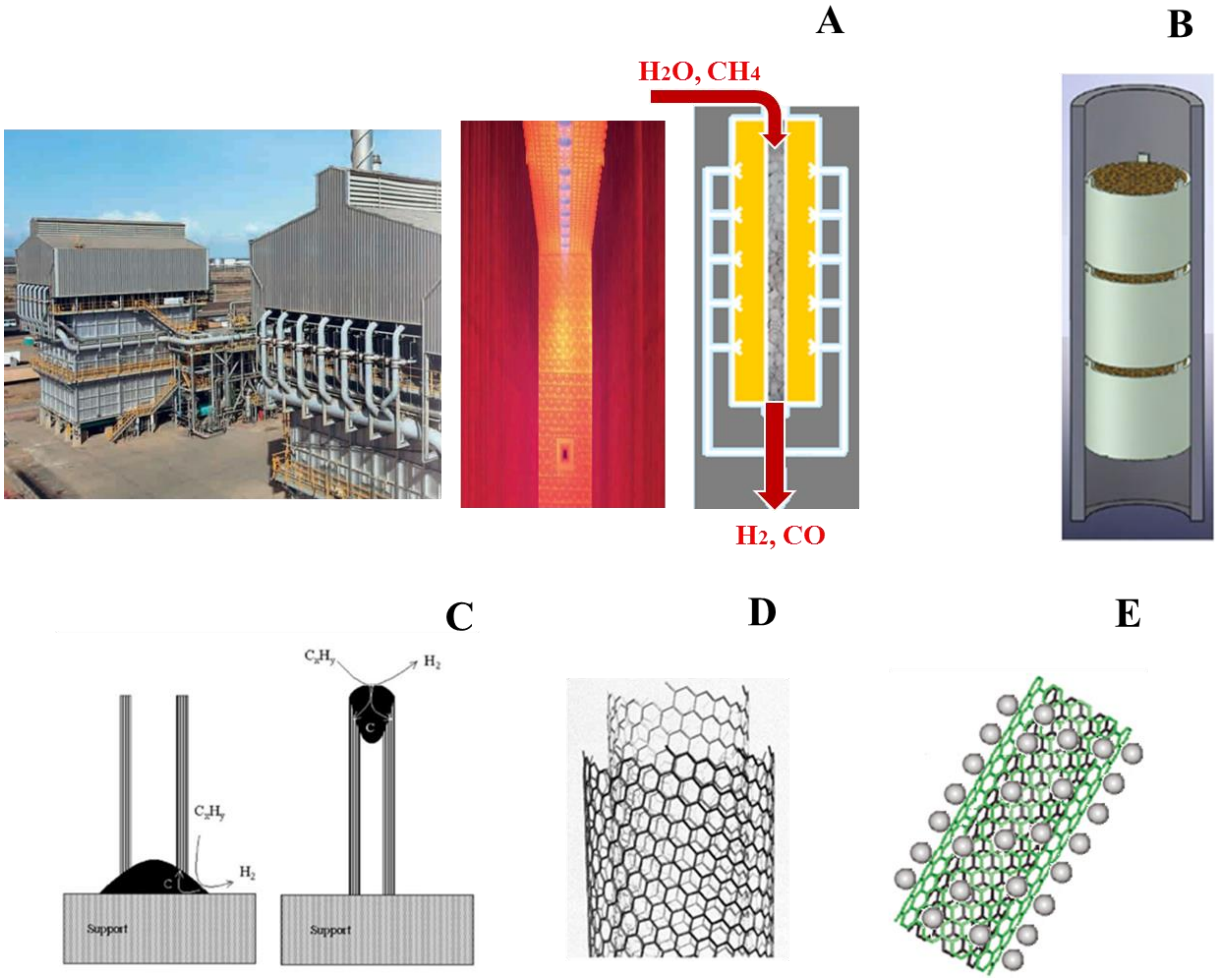

Figure 10: Overall proposed concept of structured catalyst for steam reforming: Nickel nanoparticles supported on carbon nanomaterials grown on a metal monolith. A) randomly packed pelletized catalyst in reformer tube in a typical industrial scale reformer; B) Monolithic catalytic structure in reformer tube proposed by Zamaniyan et al. (2010). Reproduced with permission from Elsevier.; C) carbon nanomaterials on monolith structure as textural promoter, grown by carbon-containing gas decomposition on metal particles (Co, Fe, Ni, etc.) (Dupuis, 2005). Reproduced with permission from Elsevier.; D) MWCNT structure as catalyst support (Peter J. F. Harris, 1999). Reproduced with permission from Cambridge University Press.; E) well dispersed Ni nanoparticles on MWCNTs.

In a typical industrial reformer, the reaction takes place in a packed bed of pelletized catalyst at an inlet temperature of 450 – 650 °C and the product gas leaves the reformer at 700 – 950 °C (Baharudin & Watson, 2017a). Ryu et al. (2007) and Basile et al. (2008) presented the application of nickel-containing catalyst supported on metal monoliths for SMR and demonstrated an enhancement of heat transfer capability in comparison with powdered catalysts that led to an improved methane conversion at a reaction temperature lower than the one used in the industrial reforming operation. Basile *et al*. demonstrated an improvement in

the methane conversion in their monolithic catalytic system at constant operating parameters (T = 900 °C; reaction duration = 12 hr; P = 20 bar; S:C = 1.7) and gas hourly space velocity (GHSV).

In the work by Ryu et al. (2007), with a flow of steam and methane (99.999 %) at a molar ratio of 3, the methane conversion was comparable (> 90%) in both the monolithic and the powdered catalysts when the GHSV was at 20,000 h^{-1}. The catalyst exit temperature was found to have been remarkably reduced by close to 200 °C in the monolithic catalyst system, from a value of approximately 900 °C in the powdered catalyst.

The lower operating temperature in the tubular reformer bed shows a promising improvement of the monolithic catalyst to not only achieve energy effective operation but also allows the potential use of the carbon nanomaterials as the textural promoter in the monolithic support system as a result of potential coke formation avoidance. A reactor design and process parameter study is of course required in order to achieve the optimal operating conditions by manipulating the feedstock gas flow rate, reaction duration, operating temperature and S:C ratio to achieve conditions under which the risk of formation of both pyrolytic and whisker coke is completely eliminated. IF such optimal reactor design and operating conditions could be achieved, the need to manipulate the operating conditions for a decoking of excessive carbon deposits *via* more aggressive gasification will be no longer necessary and hence, the risk (if any) of parallel gasification of the carbon nanomaterials-based support will be also eliminated.

We discuss earlier the potential of the application of carbon nanomaterials grown on the metal monolith as an alternative textural promoter to the conventional oxide washcoat layer that suffers from the poor adhesion with the monolith. The carbon nanomaterials however may or may not survive in the reactive conditions with regards to their chemical stability. Therefore, an idea of using the carbon nanomaterials as a removable template to synthesize a catalytic oxide layer on the overall monolithic composite presents another promising option to eliminate the risk (if any) of the carbon nanomaterials support being gasified together with the decoking of the undesired coke. Various techniques (Ajayan, Stephan, Redlich, & Colliex, 1995; Correa-Duarte et al., 2004; Muñoz-Muñoz et al., 2015; Satishkumar, Govindaraj, Nath, & Rao, 2000;

Satishkumar, Govindaraj, Vogl, Basumallick, & Rao, 1997) have been reported in the literature to synthesize the oxide nanotubes that are promising for electronics applications, but they can also be employed for our intended catalysis applications.

Conclusions

We hypothesise that the carbon nanomaterials have the desired mechanical properties and chemical/thermal stability to sustain in a properly controlled steam reforming condition. Their thermal properties make the conductive heat transport effective for the highly endothermic reaction. Their surface textural and surface modifiable properties for a good metal dispersion make them a good support for the reactant/product internal mass transfer in the diffusion-limited reaction. Although the oxygen-based functional groups grafted on the sidewall surface of the carbon nanomaterials by acid treatment may hypothetically not survive under the SMR conditions, in an oxygen-rich surface however, such oxygen groups will not be completely removed. Therefore, the nickel catalyst for the SMR reaction would hypothetically continue to have a strong interaction with the carbon nanomaterials support, but we will still need experimental evidence to investigate this.

Clean multi-walled carbon nanotubes that are of high crystallinity with well aligned vertical and parallel walls, made of graphitic sheets of hexagonally arranged carbon are expected to not only improve the mass transfer of the reacting systems due to a well-dispersed metal catalyst, but also predicted to possess a high thermal conductivity. Nanotubes growing in multiple directions produce highly interweaving structures, which introduces a greater mechanical strength of the overall composite, vital for sustainability in the harsh physical and chemical conditions of energy intensive heterogeneous reactions. Therefore, finding a balance between having high thermal conductivity (by having vertically aligned and parallel walls) and good mechanical strength (by growing nanotubes in changing directions that produce interweaving structures), is crucial. However, this is not an ultimate conclusion as there have never been any comparisons made in a single study to demonstrate the homogeneity of the metal catalyst dispersion on carbon nanofibers, single-walled carbon nanotubes and multi-walled carbon nanotubes. In addition, for a concrete finding to be established, the characterizations of the

thermal and the mechanical properties of the various carbon nanomaterial structures and their varying morphology and crystallinity qualities (defected/non-defected) need to be performed.

The deactivation of the nickel-based catalysts in steam reforming operation by coke formation is undeniable due to thermodynamics and active interaction between the metal particle surface and the carbon-containing gas, but coke deposition is avoidable and it could be removed if formed, by altering operating conditions. Alleviating the formation of the undesired coke deposition from a surface chemistry standpoint has been one of the research focuses, indicating that an optimization of the catalysts' formulation performed at the synthesis stage plays a key role. This includes optimizing the nickel crystallite size, use of other metals to replace nickel or as dopants for a bi-metallic catalyst system, and investigation of alkali doping of various oxide supports to neutralize the acidic sites on support that promote formation of coke.

Accelerating the coke gasification by increasing the steam to carbon ratio to above its stoichiometric in an attempt to decoke has been the practice in the industrial operating guideline. However, this raises question regarding the suitability for an adoption of the carbon nanomaterials as the textural promoter on metal monoliths, since the coke gasification conditions are risking a parallel gasification of the carbon support, which could lead to nickel particles sintering and hence, deactivate the catalyst due to loss of active surface area.

Based on sufficient evidence from the literature, the indications in these articles leave an open door to the possibility of the carbon nanomaterials' survival in high temperature applications, in catalytic environment and in presence of steam. We believe that highly ordered and graphitized, purified carbon nanomaterials could maintain their stability under steam-rich reforming operating conditions without being gasified (*cf.* gasification of the amorphous coke (disordered carbon)), but an experimental validation needs to be undertaken.

However, it is still best to avoid the coke formation in the first place. Achieving a balance between formation of the carbide species at the active surface of metal and their gasification at equilibrium is possible. Yet, an alternative approach could involve use of the carbon

nanomaterials grown directly on the monolithic structure as sacrificial templates for growth of the highly porous oxide support firmly attached to the monolithic, eliminating any risk of the catalyst structure collapse due to gasification of the nanostructured carbon materials.

The proposed concept of the direct growth of carbon nanomaterials on a metal monolith as a complete package of a textured catalytic support system for steam reforming could suppress the coke formation as the monolithic system has the potential to enhance the heat transfer in the reformer. Proposed nano-carbon textured monolithic system enhances the heat conduction within the reformer, making it plausible to achieve an optimal operating temperature under which the formation of both pyrolytic amorphous carbon and the growth of new highly anisotropic carbonaceous deposits (whisker coke, could have different degree of graphitization/order depending on conditions) is not favored. A reactor design and process parameter optimization study is still necessary to pinpoint operating conditions such as the feedstock gas flow rate, reaction duration, operating temperature and pressure, as well as S:C ratio required to prevent formation of both pyrolytic and whisker coke.

Acknowledgement

The authors acknowledge the financial support of the Department of Chemical and Process Engineering, University of Canterbury (UC), Christchurch, New Zealand. We would also like to express our gratitude to Professor Susan Krumdieck of the Department of Mechanical Engineering, UC for her sharing on the employment of pulsed pressure chemical vapour deposition technique in synthesizing carbon nanomaterials.

References

Abbaslou, R. M. M., Tavassoli, A., Soltan, J., & Dalai, A. K. (2009). Iron catalysts supported on carbon nanotubes for Fischer–Tropsch synthesis: Effect of catalytic site position. *Applied Catalysis A: General, 367*(1), 47-52.

Adegbite, S. (2012). Measuring the adhesion of alumina coatings onto Fecralloy supports using a mechanical testing system: North-Holland.

Agrafiotis, C., & Tsetsekou, A. (2000a). The effect of powder characteristics on washcoat quality. Part I: Alumina washcoats. *Journal of the European Ceramic Society, 20*(7), 815-824.

Agrafiotis, C., & Tsetsekou, A. (2000b). The effect of powder characteristics on washcoat quality. Part II: Zirconia, titania washcoats—multilayered structures. *Journal of the European Ceramic Society, 20*(7), 825-834.

Agrafiotis, C., Tsetsekou, A., & Ekonomakou, A. (1999). The effect of particle size on the adhesion properties of oxide washcoats on cordierite honeycombs. *Journal of materials science letters, 18*(17), 1421-1424.

Ajayan, P., Stephan, O., Redlich, P., & Colliex, C. (1995). Carbon nanotubes as removable templates for metal oxide nanocomposites and nanostructures. *Nature, 375*(6532), 564.

Almeida, L., Echave, F., Sanz, O., Centeno, M., Odriozola, J., & Montes, M. (2010). Washcoating of metallic monoliths and microchannel reactors *Studies in Surface Science and Catalysis* (Vol. 175, pp. 25-33): Elsevier.

Baharudin, L., & Watson, M. J. (2017a). Hydrogen applications and research activities in its production routes through catalytic hydrocarbon conversion. *Reviews in Chemical Engineering, 34*(1), 43-72.

Baharudin, L., & Watson, M. J. (2017b). Monolithic substrate support catalyst design considerations for steam methane reforming operation. *Reviews in Chemical Engineering, 34*(4), 481-501.

Baird, T., Fryer, J. R., & Grant, B. (1974). Carbon formation on iron and nickel foils by hydrocarbon pyrolysis—reactions at 700°C. *Carbon, 12*(5), 591-602.

Baker, R., & Sherwood, R. (1981). Catalytic gasification of graphite by nickel in various gaseous environments. *Journal of Catalysis, 70*(1), 198-214.

Baker, R. T. K. (1989). Catalytic growth of carbon filaments. *Carbon, 27*(3), 315-323. Barreto, L., Makihira, A., & Riahi, K. (2003). The hydrogen economy in the 21st century: a

sustainable development scenario. *International Journal of Hydrogen Energy*, *28*(3), 267-284.

Bartholomew, C. H. (1982). Carbon deposition in steam reforming and methanation. *Catalysis Reviews Science and Engineering, 24*(1), 67-112.

Bartholomew, C. H., & Farrauto, R. J. (2006). Hydrogen production and synthesis gas reactions *Fundamentals of Industrial Catalytic Processes, Second Edition* (Second Edition ed., pp. 339-486): John Wiley & Sons, Inc.

Basahel, S. N., Al Thabaiti, S. A., Obaid, A. Y., Mokhtar, M., & Salam, M. A. (2009). Chemical modification of multi-walled carbon nanotubes using different oxidising agents: optimisation and characterisation. *International Journal of Nanoparticles, 2*(1-6), 200-208.

Basile, F., Benito, P., Del Gallo, P., Fornasari, G., Gary, D., Rosetti, V., . . . Vaccari, A. (2008). Highly conductive Ni steam reforming catalysts prepared by electrodeposition. *Chemical Communications*(25), 2917-2919.

Beebe Jr, T. P., Goodman, D. W., Kay, B. D., & Yates Jr, J. T. (1987). Kinetics of the activated dissociative adsorption of methane on the low index planes of nickel single crystal surfaces. *The Journal of chemical physics, 87*(4), 2305-2315.

Beguin, F. F., E.; Linares-Solano, A.; Pinson, J. (2006). Surface Properties, Porosity, Chemical and Electrochemical Applications. In A. L. Loiseau, P.; Petit, P.; Roche, S.; Salvetat, J.P. (Ed.), *Understanding Carbon Nanotubes: From Basics to Applications* (pp. 495). The Netherlands: Springer, Berlin Heidelberg.

Bengaard, H. S., Nørskov, J. K., Sehested, J., Clausen, B., Nielsen, L., Molenbroek, A., & Rostrup-Nielsen, J. (2002). Steam reforming and graphite formation on Ni catalysts. *Journal of Catalysis, 209*(2), 365-384.

Berenguer, A., Cantoro, M., Golovko, V. B., Hofmann, S., Wirth, C., Johnson, B., & Robertson, J. (2009). Stable colloidal Co–Pd nanocatalysts for carbon nanotube growth. *physica status solidi (b), 246*(11-12), 2436-2439.

Boger, T., & Heibel, A. K. (2005). Heat transfer in conductive monolith structures. *Chemical Engineering Science, 60*(7), 1823-1835.

Busse, C., Freund, H., & Schwieger, W. (2018). Intensification of heat transfer in catalytic reactors by additively manufactured periodic open cellular structures (POCS). *Chemical Engineering and Processing-Process Intensification, 124*, 199-214.

Chen, D., Christensen, K. O., Ochoa-Fernández, E., Yu, Z., Tøtdal, B., Latorre, N., . . . Holmen, A. (2005). Synthesis of carbon nanofibers: effects of Ni crystal size during methane decomposition. *Journal of Catalysis, 229*(1), 82-96.

Chen, J., Yao, B., Li, C., & Shi, G. (2013). An improved Hummers method for eco-friendly synthesis of graphene oxide. *Carbon, 64*, 225-229.

Chinthaginjala, J. K., Bitter, J. H., & Lefferts, L. (2010). Thin layer of carbon-nano-fibers (CNFs) as catalyst support for fast mass transfer in hydrogenation of nitrite. *Applied Catalysis A: General, 383*(1–2), 24-32.

Chinthaginjala, J. K., & Lefferts, L. (2009). Influence of hydrogen on the formation of a thin layer of carbon nanofibers on Ni foam. *Carbon, 47*(14), 3175-3183.

Chinthaginjala, J. K., Seshan, K., & Lefferts, L. (2007). Preparation and Application of Carbon-Nanofiber Based Microstructured Materials as Catalyst Supports. *Industrial & Engineering Chemistry Research, 46*(12), 3968-3978. doi: 10.1021/ie061394r

Chinthaginjala, J. K., Thakur, D. B., Seshan, K., & Lefferts, L. (2008). How Carbon-Nano-Fibers attach to Ni foam. *Carbon, 46*(13), 1638-1647.

Chinthaginjala, J. K., Unnikrishnan, S., Smithers, M. A., Kip, G. A. M., & Lefferts, L. (2012). Carbon nanofiber growth on thin rhodium layers. *Carbon, 50*(3), 1434-1437.

Correa-Duarte, M. A., & Liz-Marzán, L. M. (2006). Carbon nanotubes as templates for one-dimensional nanoparticle assemblies. *Journal of Materials Chemistry, 16*(1), 22-25.

Correa-Duarte, M. A., Pérez-Juste, J., Sánchez-Iglesias, A., Giersig, M., & Liz-Marzán, L. M. (2005). Aligning Au nanorods by using carbon nanotubes as templates. *Angewandte Chemie International Edition, 44*(28), 4375-4378.

Correa-Duarte, M. A., Sobal, N., Liz-Marzán, L. M., & Giersig, M. (2004). Linear Assemblies of Silica-Coated Gold Nanoparticles Using Carbon Nanotubes as Templates. *Advanced Materials, 16*(23-24), 2179-2184.

Datsyuk, V., Kalyva, M., Papagelis, K., Parthenios, J., Tasis, D., Siokou, A., . . . Galiotis, C. (2008). Chemical oxidation of multiwalled carbon nanotubes. *Carbon, 46*(6), 833-840.

Davis, B. H. (2008). Development of the Science of Catalysis. In H. K. Gerhard Ertl, Ferdi Schuth, Jens Weitkamp (Ed.), *Handbook of Heterogeneous Catalysis* (Vol. 1, pp. 27). KGaA, Weinheim: WILEY-VCH Verlag GmbH & Co.

De Bokx, P., Kock, A. J. H., Boellaard, E., Klop, W., & Geus, J. W. (1985). The formation of filamentous carbon on iron and nickel catalysts: I. Thermodynamics. *Journal of catalysis, 96*(2), 454-467.

De Jong, K. P., & Geus, J. W. (2000). Carbon nanofibers: catalytic synthesis and applications. *Catalysis Reviews, 42*(4), 481-510.

Dimiev, A. M., & Tour, J. M. (2014). Mechanism of graphene oxide formation. *ACS nano, 8*(3), 3060-3068.

Dincer, I. (2002). Technical, environmental and exergetic aspects of hydrogen energy systems. *International Journal of Hydrogen Energy, 27*(3), 265-285.

Dreyer, D. R., Park, S., Bielawski, C. W., & Ruoff, R. S. (2010). The chemistry of graphene oxide. *Chemical Society Reviews, 39*(1), 228-240.

Dupuis, A.-C. (2005). The catalyst in the CCVD of carbon nanotubes—a review. *Progress in Materials Science, 50*(8), 929-961.

Echave, F., Sanz, O., Velasco, I., Odriozola, J., & Montes, M. (2013). Effect of the alloy on micro-structured reactors for methanol steam reforming. *Catalysis today, 213*, 145-154.

Ermakova, M., Ermakov, D. Y., & Kuvshinov, G. (2000). Effective catalysts for direct cracking of methane to produce hydrogen and filamentous carbon: Part I. Nickel catalysts. *Applied Catalysis A: General, 201*(1), 61-70.

Fee, C. (2017). 3D-printed porous bed structures. *Current Opinion in Chemical Engineering, 18*, 10-15.

Geng, J., Li, H., Golovko, V. B., Shephard, D. S., Jefferson, D. A., Johnson, B. F., . . . Ducati, C. (2004). Nickel formate route to the growth of carbon nanotubes. *The Journal of Physical Chemistry B, 108*(48), 18446-18450.

Giroux, T., Hwang, S., Liu, Y., Ruettinger, W., & Shore, L. (2005). Monolithic structures as alternatives to particulate catalysts for the reforming of hydrocarbons for hydrogen generation. *Applied Catalysis B: Environmental, 56*(1–2), 95-110.

Groppi, G., & Tronconi, E. (1996). Continuous vs. discrete models of nonadiabatic monolith catalysts. *AIChE Journal, 42*(8), 2382-2387.

Guo, X., Sun, Y., Yu, Y., Zhu, X., & Liu, C.-j. (2012). Carbon formation and steam reforming of methane on silica supported nickel catalysts. *Catalysis Communications, 19*, 61-65.

Hamilton Jr, R. F., Xiang, C., Li, M., Ka, I., Yang, F., Ma, D., . . . Holian, A. (2013). Purification and sidewall functionalization of multiwalled carbon nanotubes and resulting bioactivity in two macrophage models. *Inhalation toxicology, 25*(4), 199-210.

Han, J. (2005). Structures and Properties of Carbon Nanotubes. In M. Meyyappan (Ed.), *Carbon Nanotubes Science and Applications* (pp. 1). United States of America: CRC Press.

Harris, P. J. F. (1999). Synthesis: Preparation methods, growth mechanisms and processing techniques. In P. J. F. Harris (Ed.), *Carbon Nanotubes and Related Structures (New Materials for the Twenty-first Century)* (pp. 16). Cambridge, United Kingdon: Cambridge University Press.

Harris, P. J. F. (2009). *Carbon nanotube science: synthesis, properties and applications*: Cambridge university press.

Heck, R. M., Farrauto, R. J., & Gulati, S. T. (2009). *Catalytic air pollution control: commercial technology*. Hoboken, New Jersey: John Wiley & Sons.

Heck, R. M., Gulati, S., & Farrauto, R. J. (2001). The application of monoliths for gas phase catalytic reactions. *Chemical Engineering Journal, 82*(1–3), 149-156.

Helveg, S., Sehested, J., & Rostrup-Nielsen, J. (2011). Whisker carbon in perspective. *Catalysis today, 178*(1), 42-46.

Hou, P.-X., Liu, C., & Cheng, H.-M. (2008). Purification of carbon nanotubes. *Carbon, 46*(15), 2003-2025.

INCO Databooks. IN-519 Cast Chromium-Nickel-Niobium Heat-Resisting Steel (1976). INCO Europe Limited. Available from: https://www.nickelinstitute.org/~/media/Files/TechnicalLiterature/IN_519CastChromium_Nickel_NiobiumHeat_ResistingSteel_EngineeringProperties_4383_.ashx (accessed on 07.02.18).

Jarrah, N. A., Li, F., van Ommen, J. G., & Lefferts, L. (2005). Immobilization of a layer of carbon nanofibres (CNFs) on Ni foam: A new structured catalyst support. *Journal of Materials Chemistry, 15*(19), 1946-1953. doi: 10.1039/B416977H

Jones, G., Jakobsen, J. G., Shim, S. S., Kleis, J., Andersson, M. P., Rossmeisl, J., . . . Hinnemann, B. (2008). First principles calculations and experimental insight into methane steam reforming over transition metal catalysts. *Journal of Catalysis, 259*(1), 147-160.

Kho, E. T., Scott, J., & Amal, R. (2016). Ni/TiO2 for low temperature steam reforming of methane. *Chemical Engineering Science, 140*, 161-170.

Kim, P., Shi, L., Majumdar, A., & McEuen, P. (2001). Thermal transport measurements of individual multiwalled nanotubes. *Physical review letters, 87*(21), 215502.

Kim, T. W., Park, J. C., Lim, T.-H., Jung, H., Chun, D. H., Lee, H. T., . . . Yang, J.-I. (2015). The kinetics of steam methane reforming over a Ni/γ-Al2O3 catalyst for the development of small stationary reformers. *International Journal of Hydrogen Energy, 40*(13), 4512-4518.

Kock, A., De Bokx, P., Boellaard, E., Klop, W., & Geus, J. W. (1985). The formation of filamentous carbon on iron and nickel catalysts: II. Mechanism. *Journal of catalysis, 96*(2), 468-480.

Krumdieck, S., Kristinsdottir, A., Ramirez, L., Lebedev, M., & Long, N. (2007). Growth rate, microstructure and conformality as a function of vapor exposure for zirconia thin films by pulsed-pressure MOCVD. *Surface and Coatings Technology, 201*(22), 8908-8913.

Krumdieck, S., & Raj, R. (1999). Conversion Efficiency of Alkoxide Precursor to Oxide Films Grown by an Ultrasonic-Assisted, Pulsed Liquid Injection, Metalorganic Chemical Vapor Deposition (Pulsed-CVD) Process. *Journal of the American Ceramic Society, 82*(6), 1605-1607.

Krumdieck, S., & Raj, R. (2001). Growth rate and morphology for ceramic films by pulsed-MOCVD. *Surface and Coatings Technology, 141*(1), 7-14.

Krumdieck, S. P., & Raj, R. (2001). Experimental characterization and modeling of pulsed MOCVD with ultrasonic atomization of liquid precursor. *Chemical Vapor Deposition, 7*(2), 85-90.

Krumdieck, S. P., Sbaizero, O., Bullert, A., & Raj, R. (2002). Solid Yttria-Stabilized Zirconia Films by Pulsed Chemical Vapor Deposition from Metal-organic Precursors. *Journal of the American Ceramic Society, 85*(11), 2873-2875.

Lämmermann, M., Horak, G., Schwieger, W., & Freund, H. (2018). Periodic open cellular structures (POCS) for intensification of multiphase reactors: Liquid holdup and two-phase pressure drop. *Chemical Engineering and Processing-Process Intensification, 126*, 178-189.

Lämmermann, M., Schwieger, W., & Freund, H. (2016). Experimental investigation of gas-liquid distribution in periodic open cellular structures as potential catalyst supports. *Catalysis Today, 273*, 161-171.

Li, P., Li, T., Zhou, J.-H., Sui, Z.-J., Dai, Y.-C., Yuan, W.-K., & Chen, D. (2006). Synthesis of carbon nanofiber/graphite-felt composite as a catalyst. *Microporous and Mesoporous Materials, 95*(1–3), 1-7.

Li, Y., Zhang, B., Xie, X., Liu, J., Xu, Y., & Shen, W. (2006). Novel Ni catalysts for methane decomposition to hydrogen and carbon nanofibers. *Journal of Catalysis, 238*(2), 412-424.

López, E., Kim, J., Shanmugharaj, A., & Ryu, S. (2012). Multiwalled carbon nanotubes-supported Nickel catalysts for the steam reforming of propane. *Journal of Materials Science, 47*(6), 2985-2994.

Ma, P.-C., Siddiqui, N. A., Marom, G., & Kim, J.-K. (2010). Dispersion and functionalization of carbon nanotubes for polymer-based nanocomposites: a review. *Composites Part A: Applied Science and Manufacturing, 41*(10), 1345-1367.

Marcano, D. C., Kosynkin, D. V., Berlin, J. M., Sinitskii, A., Sun, Z., Slesarev, A., . . . Tour, J. M. (2010). Improved synthesis of graphene oxide. *ACS nano, 4*(8), 4806-4814.

Matsumura, Y., & Nakamori, T. (2004). Steam reforming of methane over nickel catalysts at low reaction temperature. *Applied Catalysis A: General, 258*(1), 107-114.

Mierczynski, P., Ciesielski, R., Kedziora, A., Nowosielska, M., Kubicki, J., Maniukiewicz, W., . . . Maniecki, T. P. (2016). Monometallic copper catalysts supported on multi-walled carbon nanotubes for the oxy-steam reforming of methanol. *Reaction Kinetics, Mechanisms and Catalysis, 117*(2), 675-691.

Mohammadzadeh, J. S., & Zamaniyan, A. (2002). Catalyst shape as a design parameter—optimum shape for methane-steam reforming catalyst. *Chemical Engineering Research and Design, 80*(4), 383-391.

Mohino, F., Martin, A. B., Salerno, P., Bahamonde, A., & Mendioroz, S. (2005). High surface area monoliths based on pillared clay materials as carriers for catalytic processes. *Applied Clay Science, 29*(2), 125-136.

Moisala, A., Nasibulin, A. G., & Kauppinen, E. I. (2003). The role of metal nanoparticles in the catalytic production of single-walled carbon nanotubes—a review. *Journal of Physics: condensed matter, 15*(42), S3011.

Moraes, R. A., Matos, C. F., Castro, E. G., Schreiner, W. H., Oliveira, M. M., & Zarbin, A. J. (2011). The effect of different chemical treatments on the structure and stability of aqueous dispersion of iron-and iron oxide-filled multi-walled carbon nanotubes. *Journal of the Brazilian Chemical Society, 22*(11), 2191-2201.

Morales-Torres, S., Pérez-Cadenas, A. F., Kapteijn, F., Carrasco-Marín, F., Maldonado-Hódar, F. J., & Moulijn, J. A. (2009). Palladium and platinum catalysts supported on carbon nanofiber coated monoliths for low-temperature combustion of BTX. *Applied Catalysis B: Environmental, 89*(3–4), 411-419.

Moseley, F., Stephens, R., Stewart, K., & Wood, J. (1972). The poisoning of a steam hydrocarbon gasification catalyst. *Journal of Catalysis, 24*(1), 18-39.

Muñoz-Muñoz, F., Soto, G., Domínguez, D., Romo-Herrera, J., Bedolla-Valdez, Z. I., Alonso-Nuñez, G., . . . Tiznado, H. (2015). The control of thickness on aluminum oxide nanotubes by Atomic Layer Deposition using carbon nanotubes as removable templates. *Powder Technology, 286*, 602-609.

Muradov, N. (2001). Catalysis of methane decomposition over elemental carbon. *Catalysis communications, 2*(3), 89-94.

Muradov, N., Smith, F., & Ali, T. (2005). Catalytic activity of carbons for methane decomposition reaction. *Catalysis Today, 102*, 225-233.

Nam, I., Lee, H., Sim, J., & Choi, S. (2012). Electromagnetic characteristics of cement matrix materials with carbon nanotubes. *ACI Materials Journal-American Concrete Institute, 109*(3), 363.

Nam, I., Souri, H., & Lee, H. (2016). Percolation threshold and piezoresistive response of multi-wall carbon nanotube/cement composites. *Smart Structures and Systems, 18*(2), 217-231.

Nijhuis, T. A., Beers, A. E., Vergunst, T., Hoek, I., Kapteijn, F., & Moulijn, J. A. (2001). Preparation of monolithic catalysts. *Catalysis Reviews, 43*(4), 345-380.

Oliveira, N. M., Valençaa, G. P., & Vieirab, R. (2015). Water Gas Shift Reaction On Copper Catalysts Supported On Alumina And Carbon Nanofibers. *Chemical Engineering, 43*.

Olivier, J., Buqa, H., Kohs, W., Schröttner, H., Golob, P., & Winter, M. (2001). The relevance of graphite surface properties for anode performance in lithium ion cells-III. Surface area and surface heterogeneieties. *Proceedings of the ABA-2, International Conference on Advanced Batteries and Accumulators, Brno (Czech Republic)*.

Olivier, J., & Winter, M. (2001). Determination of the absolute and relative extents of basal plane surface area and "non-basal plane surface" area of graphitesand their impact on anode performance in lithium ion batteries. *Journal of Power Sources, 4155*, 1-5.

Pacheco Benito, S., & Lefferts, L. (2010). The production of a homogeneous and well-attached layer of carbon nanofibers on metal foils. *Carbon, 48*(10), 2862-2872.

Pacheco Benito, S., & Lefferts, L. (2012). Influence of reaction parameters on the attachment of a carbon nanofiber layer on Ni foils. *Surface and Coatings Technology, 206*(15), 3366-3373.

Rodríguez-reinoso, F. (1998). The role of carbon materials in heterogeneous catalysis. *Carbon, 36*(3), 159-175.

Roh, H.-S., Lee, D. K., Koo, K. Y., Jung, U. H., & Yoon, W. L. (2010). Natural gas steam reforming for hydrogen production over metal monolith catalyst with efficient heat-transfer. *International Journal of Hydrogen Energy, 35*(4), 1613-1619.

Rostrup-Nielsen, J., & Trimm, D. L. (1977). Mechanisms of carbon formation on nickel-containing catalysts. *Journal of Catalysis, 48*(1-3), 155-165.

Rostrup-Nielsen, J. R. (1972). Equilibria of decomposition reactions of carbon monoxide and methane over nickel catalysts. *Journal of Catalysis, 27*(3), 343-356.

Rostrup-Nielsen, J. R. (1974). Coking on nickel catalysts for steam reforming of hydrocarbons. *Journal of Catalysis, 33*(2), 184-201.

Roy, S., Bauer, T., Al-Dahhan, M., Lehner, P., & Turek, T. (2004). Monoliths as multiphase reactors: a review. *AIChE journal, 50*(11), 2918-2938.

Ryu, J.-H., Lee, K.-Y., La, H., Kim, H.-J., Yang, J.-I., & Jung, H. (2007). Ni catalyst wash-coated on metal monolith with enhanced heat-transfer capability for steam reforming. *Journal of Power Sources, 171*(2), 499-505.

Saito, M., Kojima, J., Iwai, H., & Yoshida, H. (2015). The limiting process in steam methane reforming with gas diffusion into a porous catalytic wall in a flow reactor. *International Journal of Hydrogen Energy, 40*(29), 8844-8855.

Saito, T. (2004). Chemistry of transition metals *Inorganic Chemistry* (Online Edition ed., pp. 110-144). Japan: Iwanami Publishing Company.

Salmoria, G., Michelena, I., Barra, G., Vieira, L., & Paggi, R. (2013). *Oxidative treatment of carbon nanotubes by hydrogen peroxide and O2 plasma for rapid manufacturing applications.* Paper presented at the High Value Manufacturing: Advanced Research in Virtual and Rapid Prototyping: Proceedings of the 6th International Conference on Advanced Research in Virtual and Rapid Prototyping, Leiria, Portugal, 1-5 October, 2013.

Satishkumar, B., Govindaraj, A., Nath, M., & Rao, C. N. R. (2000). Synthesis of metal oxide nanorods using carbon nanotubes as templates. *Journal of Materials Chemistry, 10*(9), 2115-2119.

Satishkumar, B., Govindaraj, A., Vogl, E. M., Basumallick, L., & Rao, C. (1997). Oxide nanotubes prepared using carbon nanotubes as templates. *Journal of materials research, 12*(03), 604-606.

Seelam, P., Huuhtanen, M., Sápi, A., Szabó, M., Kordás, K., Turpeinen, E., . . . Keiski, R. (2010). CNT-based catalysts for H 2 production by ethanol reforming. *international journal of hydrogen energy, 35*(22), 12588-12595.

Shaikhutdinov, S. K., Avdeeva, L., Novgorodov, B., Zaikovskii, V., & Kochubey, D. (1997). Nickel catalysts supported on carbon nanofibers: structure and activity in methane decomposition. *Catalysis letters, 47*(1), 35-42.

Sinha, S., Barjami, S., Iannacchione, G., Schwab, A., & Muench, G. (2005). Off-axis thermal properties of carbon nanotube films. *Journal of Nanoparticle Research, 7*(6), 651-657.

Siriwongrungson, V., Alkaisi, M. M., & Krumdieck, S. P. (2007). Step coverage of thin titania films on patterned silicon substrate by pulsed-pressure MOCVD. *Surface and Coatings Technology, 201*(22), 8944-8949.

Špitalský, Z., Krontiras, C. A., Georga, S. N., & Galiotis, C. (2009). Effect of oxidation treatment of multiwalled carbon nanotubes on the mechanical and electrical properties of their epoxy composites. *Composites Part A: Applied Science and Manufacturing, 40*(6), 778-783.

Stancu, M., Ruxanda, G., Ciuparu, D., & Dinescu, A. (2011). Purification of multiwall carbon nanotubes obtained by AC arc discharge method. *Optoelectronics and Advanced Materials, 5*(8), 846-850.

Suelves, I., Pinilla, J., Lázaro, M., & Moliner, R. (2008). Carbonaceous materials as catalysts for decomposition of methane. *Chemical Engineering Journal, 140*(1), 432-438.

Taha, T. J., Mojet, B. L., Lefferts, L., & van der Meer, T. H. (2016). Effect of carbon nanofiber surface morphology on convective heat transfer from cylindrical surface: Synthesis, characterization and heat transfer measurement. *International Journal of Thermal Sciences, 105*, 13-21.

Teo, K. B., Singh, C., Chhowalla, M., & Milne, W. I. (2003). Catalytic synthesis of carbon nanotubes and nanofibers. In H. S. Nalwa (Ed.), *Encyclopedia of nanoscience and nanotechnology (Vol. 10)* (Vol. 10, pp. 1-22). USA: American Scientific Publishers.

Tobias, G., Shao, L., Salzmann, C. G., Huh, Y., & Green, M. L. (2006). Purification and opening of carbon nanotubes using steam. *The Journal of Physical Chemistry B, 110*(45), 22318-22322.

Tonkovich, A. Y., Perry, S., Wang, Y., Qiu, D., LaPlante, T., & Rogers, W. A. (2004). Microchannel process technology for compact methane steam reforming. *Chemical Engineering Science, 59*(22–23), 4819-4824.

Tribolet, P., & Kiwi-Minsker, L. (2005). Palladium on carbon nanofibers grown on metallic filters as novel structured catalyst. *Catalysis Today, 105*(3–4), 337-343.

Trimm, D. L. (1997). Coke formation and minimisation during steam reforming reactions. *Catalysis Today, 37*(3), 233-238.

Trimm, D. L. (1999). Catalysts for the control of coking during steam reforming. *Catalysis Today, 49*(1), 3-10.

Tronconi, E., Groppi, G., & Visconti, C. G. (2014). Structured catalysts for non-adiabatic applications. *Current Opinion in Chemical Engineering, 5*, 55-67.

Tuzovskaya, I., Pacheco Benito, S., Chinthaginjala, J. K., Reed, C., Lefferts, L., & van der Meer, T. (2012). Heat exchange performance of stainless steel and carbon foams modified with carbon nano fibers. *International Journal of Heat and Mass Transfer, 55*(21–22), 5769-5776.

Twigg, M., & Richardson, J. (2002). Theory and applications of ceramic foam catalysts. *Chemical Engineering Research and Design, 80*(2), 183-189.

Wu, H., La Parola, V., Pantaleo, G., Puleo, F., Venezia, A. M., & Liotta, L. F. (2013). Ni-based catalysts for low temperature methane steam reforming: recent results on Ni-Au and comparison with other bi-metallic systems. *Catalysts, 3*(2), 563-583.

Wunderlich, W. T., M. (2006). Plasma-CVD Growth of Carbon nano-Tubes on Metal Substrates. In D. A. Martin (Ed.), *Trends in Nanotubes Research*. New York: Nova Science Publishers.

Xia, W., Hagen, V., Kundu, S., Wang, Y., Somsen, C., Eggeler, G., . . . Muhler, M. (2007). Controlled Etching of Carbon Nanotubes by Iron-Catalyzed Steam Gasification. *Advanced Materials, 19*(21), 3648-3652.

Xu, J., & Froment, G. F. (1989). Methane steam reforming, methanation and water-gas shift: I. Intrinsic kinetics. *AIChE journal, 35*(1), 88-96.

Yang, F., Wang, X., Si, J., Zhao, X., Qi, K., Jin, C., . . . Yang, J. (2016). Water-assisted preparation of high-purity semiconducting (14, 4) carbon nanotubes. *ACS nano, 11*(1), 186-193.

Yang, H.-M., & Liao, P.-H. (2007). Preparation and activity of Cu/ZnO-CNTs nano-catalyst on steam reforming of methanol. *Applied Catalysis A: General, 317*(2), 226-233.

Zamaniyan, A., Khodadadi, A. A., Mortazavi, Y., & Manafi, H. (2011). Comparative model analysis of the performance of tube fitted bulk monolithic catalyst with conventional pellet shapes for natural gas reforming. *Journal of Industrial and Engineering Chemistry, 17*(4), 767-776.

Zamaniyan, A., Mortazavi, Y., Khodadadi, A. A., & Manafi, H. (2010). Tube fitted bulk monolithic catalyst as novel structured reactor for gas–solid reactions. *Applied Catalysis A: General, 385*(1–2), 214-223.

Zhang, T., & Amiridis, M. D. (1998). Hydrogen production via the direct cracking of methane over silica-supported nickel catalysts. *Applied Catalysis A: General, 167*(2), 161-172.

Zhu, J., Jia, Y., Li, M., Lu, M., & Zhu, J. (2013). Carbon Nanofibers Grown on Anatase Washcoated Cordierite Monolith and Its Supported Palladium Catalyst for Cinnamaldehyde Hydrogenation. *Industrial & Engineering Chemistry Research, 52*(3), 1224-1233.